

Article

Hydrochemical Characterization of Surface Water and Groundwater in the Crystalline Basement Aquifer System in the Pra Basin (Ghana)

Evans Manu ^{1,2,*} , Marco De Lucia ¹  and Michael Kühn ^{1,2} 

¹ GFZ German Research Centre for Geosciences, Fluid Systems Modelling, Telegrafenberg, 14473 Potsdam, Germany

² Institute of Geosciences, University of Potsdam, Karl-Liebknecht-Str. 24-25, 14476 Potsdam-Golm, Germany

* Correspondence: evans.manu@gfz-potsdam.de

Abstract: The quality of groundwater resources in the Pra Basin (Ghana) is threatened by ongoing river pollution from illegal mining. To date, there are very limited data and literature on the hydrochemical characteristics of the basin. For the first time, we provide regional hydrochemical data on surface water and groundwater to gain insight into the geochemical processes and quality for drinking and irrigation purposes. We collected 90 samples from surface water (rivers) and groundwater (boreholes) and analysed them for their chemical parameters. We performed a water quality assessment using conventional water quality rating indices for drinking water and irrigation. Cluster and factor analysis were performed on the hydrochemical data to learn the chemical variations in the hydrochemical data. Bivariate ion plots were used to interpret the plausible geochemical processes controlling the composition of dissolved ions in surface water and groundwater. The water quality assessment using Water Quality Index (WQI) revealed that 74% of surface water and 20% of groundwater samples are of poor drinking quality and, therefore, cannot be used for drinking purposes. For irrigation, surface water and groundwater are of good quality based on Sodium Adsorption Ratio (SAR), Wilcox diagram and United States Salinity (USSS) indices. However, Mn and Fe (total) concentrations observed in most surface water samples are above the acceptable limit for irrigation and therefore require treatment to avoid soil acidification and loss of availability of vital soil nutrients. Manganese and iron (total) are identified as the main contaminants affecting the basin's water quality. The hierarchical cluster analysis highlights the heterogeneity in the regional hydrochemical data, which showed three distinct spatial associations based on elevation differences. Groundwater composition chemically evolves from a Ca-HCO₃ to a Na-HCO₃ and finally to a Na-Cl water type along the flow regime from the recharge to the discharge zone. The bivariate ion plot and the factor analysis underscore silicate weathering, carbonate dissolution and ion exchange as the most likely geochemical processes driving the hydrochemical evolution of the Pra Basin groundwater. Going forward, geochemical models should be implemented to elucidate the dominant reaction pathways driving the evolution of groundwater chemistry in the Pra Basin.

Keywords: water quality; cluster analysis; mining; hydrochemical evolution; silicate weathering



Citation: Manu, E.; De Lucia, M.; Kühn, M. Hydrochemical Characterization of Surface Water and Groundwater in the Crystalline Basement Aquifer System in the Pra Basin (Ghana). *Water* **2023**, *15*, 1325. <https://doi.org/10.3390/w15071325>

Academic Editors: Fuhong Sun and Fanhao Song

Received: 2 March 2023

Revised: 22 March 2023

Accepted: 26 March 2023

Published: 28 March 2023



Copyright: © 2023 by the authors. Licensee MDPI, Basel, Switzerland. This article is an open access article distributed under the terms and conditions of the Creative Commons Attribution (CC BY) license (<https://creativecommons.org/licenses/by/4.0/>).

1. Introduction

One of the components of the United Nations sustainable development goals is ensuring access to quality water and improved sanitation for all [1]. This has become necessary due to the increasing pollution of large surface water bodies and the complex nature of some aquifers around the world [2–5]. The problem of unregulated anthropogenic activities, such as poor agricultural practices, illegal mining and indiscriminate sewage disposal are major causes of water pollution, especially in many parts of Africa. According to the United Nations, more than 80% of human waste is discharged into rivers untreated, and more than 40% of the world's population is affected by water scarcity [1]. The situation is

worst in many developing countries, such as Ghana. One of the river basins affected by these activities is the Pra Basin in Ghana. Over the past decade, large river networks that provide water to over four million people have been adversely affected by illegal mining activities [6–11]. This new development has increased dependence on groundwater as the only available alternative source of water supply. Specific uses of the groundwater in the basin include drinking, industrial, animal watering and mechanized irrigation systems that require good quality for their applications. Therefore, determining the geochemical processes that control the evolution of groundwater and its quality is essential [12–14] to ensure sustainable water resource management in the basin.

Groundwater is protected from contamination by anthropogenic pollutants due to the filtering capacity of the overburden material and is therefore usually preferred to surface water [15]. However, the quality may deteriorate depending on the local environmental conditions [16–18]. Several factors contribute to changes in groundwater hydrochemistry, including climate, precipitation, mineralogy of the underlying geology with which the water interacts, aquifer properties and topography. These factors contribute to the spatial and temporal changes in the water composition. Understanding the hydrochemical characteristics of groundwater thus provides insight into the mechanisms and geochemical processes that drive groundwater chemical evolution.

In the study area, research on the hydrochemical characterization of surface water and groundwater is very sparse and the few ones that exist [19–21] are poorly coordinated to provide a regional overview for better planning and management of the aquifers in the basin. The complexity characterizing the underlying geology and the enormous land-use changes make it very difficult to understand the processes that determine the quality of surface water and groundwater in a regional setting.

Several researchers have used various conventional approaches to assess the quality of water resources for drinking [22–24] and irrigation [21,25] purposes. The Water Quality Index (WQI) has been used extensively in various geological terrains to study surface water and groundwater quality for drinking [26,27]. Others have been employed to study irrigation water quality, including the USSL, %Na and Wilcox diagram [21,25,28]. In the Pra Basin, Loh et al. [21] used the WQI, %Na, Wilcox and the United States Salinity Level diagram to assess groundwater quality in the Lake Bosumtwi area of the Pra Basin and concluded that the groundwater is of good quality for drinking and irrigation and demonstrated the utility of these approaches in studying water quality in the terrain.

In the present study, major ions and trace metals are used to provide knowledge about spatial variation in surface water and groundwater quality and geochemical processes in the Pra Basin of Ghana. We deduce the important geochemical processes that govern the evolution of groundwater composition in the basin. Here we employed classical methods, including WQI, %Na, USSL and Wilcox diagram, to assess the water quality for drinking and irrigation. Hierarchical cluster analysis (HCA) was used to establish spatial associations within the hydrochemical dataset. Factor analysis was used to reduce the dimensionality of the data to identify the plausible factors driving groundwater chemical evolution.

2. Materials and Methods

2.1. Location and Physical Setting

The study area (Figure 1A) is in the Pra Basin in Ghana (Figure 1B,C). It is one of the basins with an established management board set up by the Water Resources Commission (WRC). The study area lies between the Universal Transverse Mercator (UTM) coordinates 30 N 795,477m E, 30 N 624,441m E and 30 N 553,263m N, 30 N 744,975m N. The catchment area consists of the Birim and the main Pra rivers. It covers a total area of about 10,703 km² [29]. The rivers are perennial and cross several towns and serve as the main source of water supply for many communities and industries within the basin. However, recent activities, including illegal mining, have rendered many of these rivers undrinkable, making the groundwater resource the most reliable for water supply [6–11].

The main economic activities in the study area are mining and agriculture. It is estimated that over 60% of the people are engaged in agriculture [29], with cocoa cultivation being the predominant agricultural activity in the region. Large-scale mining activities have been conducted since the 1950s, however, illegal mining has recently increased throughout the basin in search of economic minerals such as gold, bauxite, diamonds, manganese and iron.

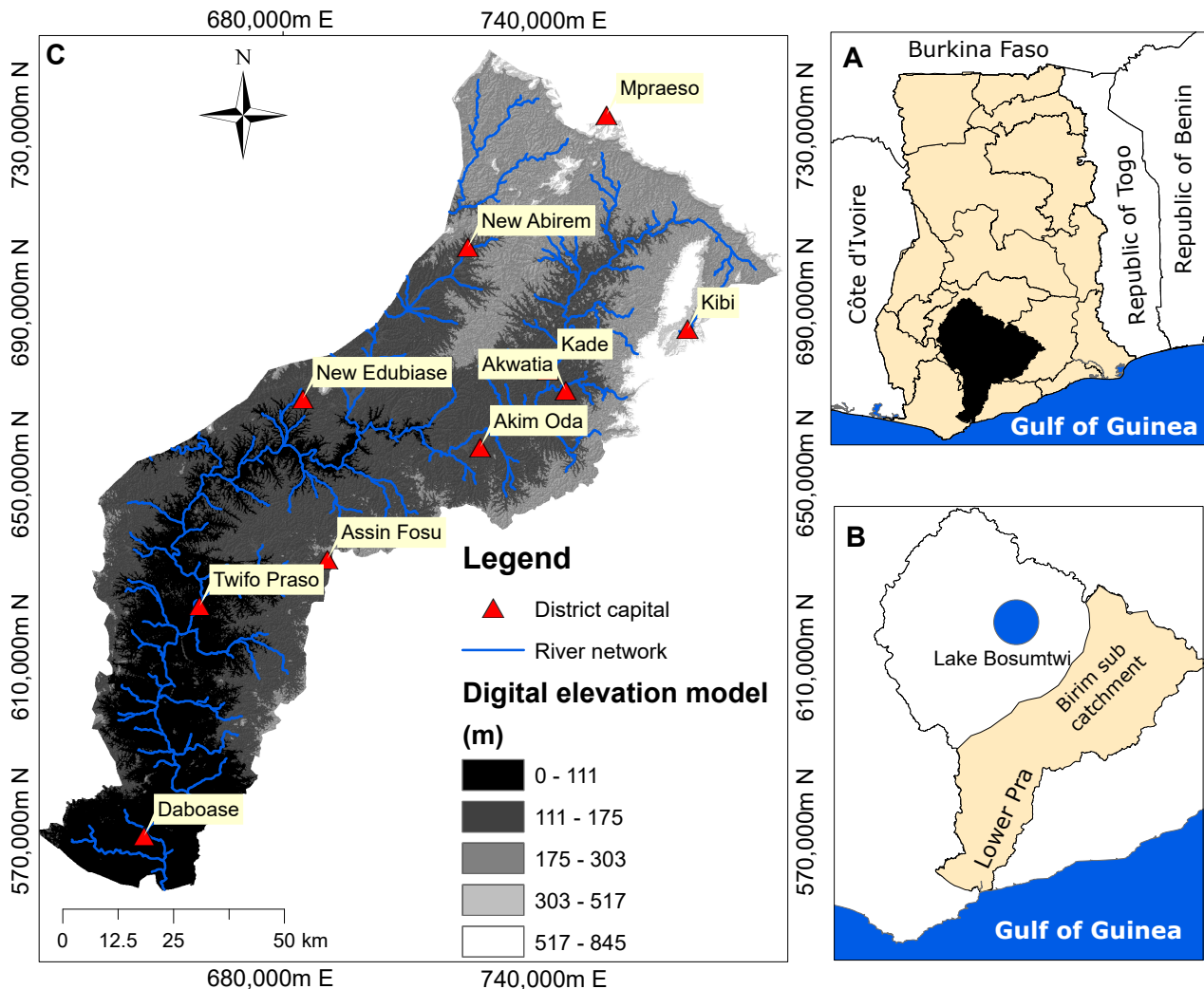


Figure 1. The location of the main Pra Basin in Ghana and the international boundaries (A), the study area representing the Birim and the Lower Pra catchments of the Pra Basin (B), the digital elevation model (DEM) of the study area and the river networks, including some notable districts (C).

2.2. Geology

The study area consists of two major rock formations, the Birimian Supergroup and the Cape Coast granitoid complex (Figure 2). The Birimian underlies the northern area, and the Cape Coast granitoid mostly the southern area. There is also the Tarkwain Formation, which is found in a few areas on the eastern and western edges of the study area. The Birimian consists mainly of meta-sediments and includes phyllite, shale and greywacke. On top of the Birimian lies the Tarkwain Formation, which consists of sandstones, conglomerates and argillites. The Cape Coast granitoid is massive and outcrops predominantly in Ghana’s southern parts [30,31]. The Cape Coast type granite comprises quartz, gneiss, foliated biotite and horn–blende–quartz–diortite gneiss [32].

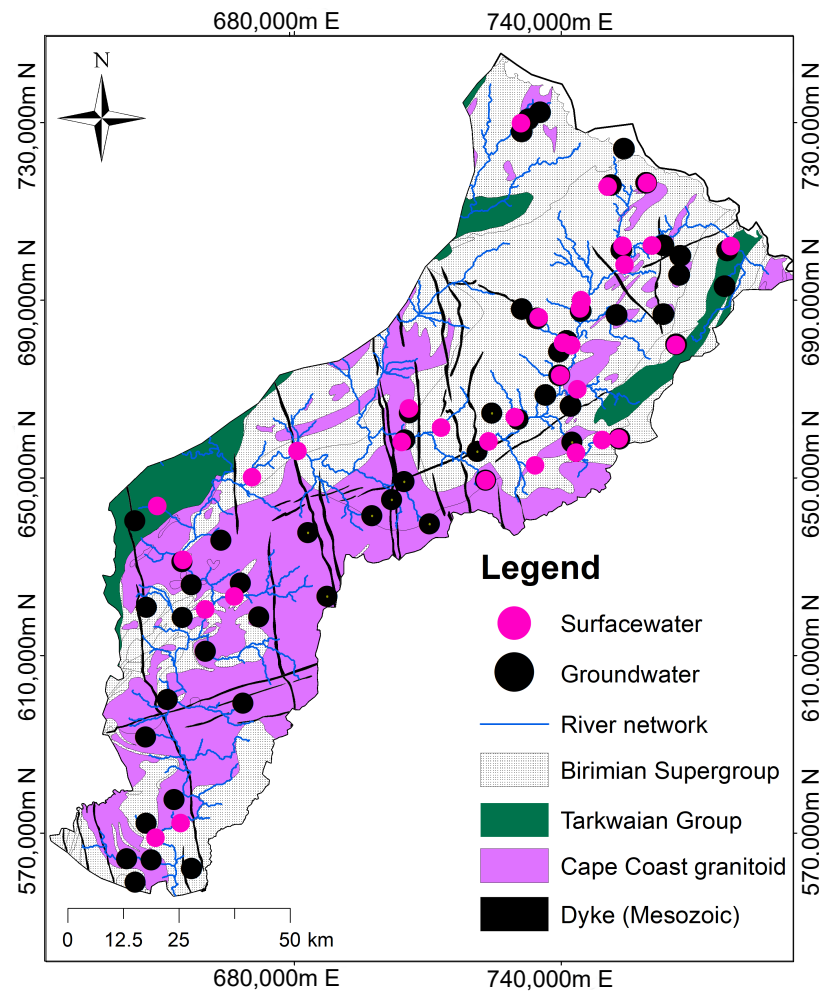


Figure 2. Geological map of the study area showing the predominant rock types and the sampling locations. The Birimian Supergroup consist of meta-sediments, mainly phyllite, schists and greywacke. The Tarkwaian Group consist of sandstones, conglomerates and argillites, the Cape Coast granitoid of quartz and dioritic gneiss and the Dyke is made of dolerite.

2.3. Surface Water and Groundwater Sampling

A total of 90 water samples were taken from rivers ($n = 34$) and boreholes ($n = 56$) in the study area. The sampling wells were selected taking into account geology, accessibility and spatial distribution (Figure 2). The sampling was carried out in March 2020. The sampling campaign coincided with the start of the major rainy season, which begins in mid-March and early April. Temperatures during the sampling period ranged from 27 to 30 °C, with a mean of 28 °C. Prior to sampling, the boreholes were first flushed for a minimum of 15 min to remove stagnant water and ensured representative water from the aquifer was reached. A detailed description about materials and sampling procedure are elaborated in Manu et al. [33].

2.4. Instrumentation and Measurements

The concentrations of cations (Na^+ , K^+ , Ca^{2+} and Mg^{2+}) and trace metals (Si, Ba, Mn and Fe) were measured by Inductively Coupled Plasma Optical Emission Spectrometry (ICP-OES). The anion concentrations (Cl^- , HCO_3^- , SO_4^{2-} , NO_3^-) were measured by ion chromatography (ICS 3000, Thermo Fisher Scientific, Waltham, MA, USA) using an AS11 HC column and a conductivity detector. The analytical precision of the ICP-OES and IC was $\pm 5\%$. Parameters including pH, dissolved oxygen (DO), electrical conductivity (EC) and temperature, were determined in the field using the WTW profiline 3320 series

multi-parameter measuring device. Alkalinity (as HCO_3^-) measurements were carried out onsite via HACH digital Titrator Model 16900.

To ensure the reliability of the measurements, duplicate samples of some of the rivers and boreholes were collected, and measurements were conducted to cross-check their corresponding measured samples. The final measurements were subjected to an internal consistency test using percentage charge balance error (CBE). In this study, a $\text{CBE} < \pm 3\%$ was achieved and considered sufficient.

2.5. Computation of Water Quality Indices

The sodium adsorption ratio (SAR) and the water quality index (WQI) were calculated from the hydrochemical data to assess the quality of the water for irrigation and drinking purposes. A total of 11 chemical parameters including Na^+ , K^+ , Ca^{2+} , Mg^{2+} , Cl^- , HCO_3^- , SO_4^{2-} , NO_3^- , Ba, Mn and Fe (total) were used to calculate the WQI of the water samples. The computation of the WQI involved four steps [34]. In the first step, all chemical parameters were assigned weights (w_i) according to their negative impact on human health with reference to the WHO guideline protocol for drinking water [35]. In step two, the relative weight ($W_i = w_i / \sum w_i$) of each parameter was calculated. The WHO standard for the parameters in drinking water [35], their assigned weights and calculated relative weights are presented in Table 1. Step 3 involved calculating the quality rating scale (q_i), as shown in Equation (1):

$$q_i = \frac{C_i}{S_i} \times 100 \quad (1)$$

where q_i , C_i and S_i are the quality rating value, the concentration of each parameter and the WHO standard values of each parameter, respectively. Finally, the WQI was computed using Equation (2):

$$\text{WQI} = \sum W_i \times q_i \quad (2)$$

The WQI classification scheme by Sahu and Sikdar [34] was used to interpret the threshold values acceptable for drinking purposes. The drinking water classification scheme includes excellent water ($\text{WQI} < 50$), good water (WQI between 50 and 100), poor water (WQI between 100 and 200), very poor water (WQI between 200 and 300) and not suitable for drinking ($\text{WQI} > 300$).

Table 1. List of parameters used to calculate the WQI, their standard drinking water reference values [35], for drinking water, assigned weights (w_i) and relative weights (W_i).

Parameter	Standard [35]	Weight (w_i)	Relative Weight (W_i)
pH	7.5	4	0.138
Na^+	200	2	0.069
Ca^{2+}	200	2	0.069
Mg^{2+}	150	2	0.069
Cl^-	250	3	0.103
SO_4^{2-}	250	3	0.103
NO_3^-	10	5	0.172
Mn	0.1	3	0.103
Fe	0.3	3	0.103
Ba	1.3	2	0.069
Total		29	1.0

Note(s): All concentrations are in mg/L except pH.

The SAR was calculated using the equation proposed by Allison and Richards [36] and Hem [37] which is contained in Equation (3):

$$\text{SAR} = \frac{\text{Na}^+}{\sqrt{\frac{\text{Ca}^{2+} + \text{Mg}^{2+}}{2}}} \quad (3)$$

Ion concentration in meq/L was adopted for the calculation.

The Wilcox plot was generated by plotting EC vs. %Na⁺. The %Na⁺ was calculated using Equation (4):

$$\%Na^+ = \frac{Na^+ + K^+}{Ca^{2+} + Mg^{2+} + Na^+ + K^+} \times 100 \quad (4)$$

All ion concentrations are expressed in meq/L.

The USSL diagram was created by plotting the EC against the SAR. The interpretation of irrigation quality from the USSL was based on four classifications, categorized as low, medium, high and very high salinity levels. Water samples falling within the low and medium salinity areas in the plot are considered excellent to good for irrigation.

The chloro-alkali indices were used to study the occurrence of cation exchange in groundwater. Schoeller [38] proposed two chloro-alkali indices, CAI-I and CAI-II, to assess the presence of such processes in groundwater. The two indices are calculated using Equations (5) and (6), respectively:

$$CAI - I = \frac{Cl^- - (Na^+ + K^+)}{Cl^-} \quad (5)$$

$$CAI - II = \frac{Cl^- - (Na^+ + K^+)}{CO_3^{2-} + SO_4^{2-} + HCO_3^- + NO_3^-} \quad (6)$$

All ion concentrations are taken in meq/L. The chloro-alkali indices < 0 indicate the occurrence of cation exchange and >0 emphasize reverse ion exchange.

2.6. Cluster Analysis of the Groundwater Hydrochemical Data

The groundwater hydrochemical data were subjected to multivariate statistical analysis to learn about the spatial associations and factors controlling groundwater chemistry. The data were logarithmically transformed and standardized to their respective z-scores to ensure that all hydrochemical data met the requirements of normal distribution. Factor analysis with the principal component as the extraction criterion was applied to the transformed data (z-scores) to reduce the data in order to establish the relationship between the variables. To optimize the variations between the variables, we used the varimax rotation method to ensure that the data are uncorrelated. The Kaiser Criterion [39] was applied to remove components that do not provide unique processes in the hydrochemistry. Factors that loaded communalities < 0.5 were excluded from the analysis and the process repeated. The reason for this is that variables that load communalities < 0.5 do not show much influence among generated principal components and, therefore contribute only marginally to the factor model [40].

The hierarchical cluster analysis (HCA) was used to partition the hydrochemical data based on their spatial correlation. Here all the standardized (z-score) hydrochemical parameters including pH, Na⁺, K⁺, Ca²⁺, Mg²⁺, Cl⁻, HCO₃⁻, SO₄²⁻, NO₃⁻, Ba, Mn and Fe (total) were included in the HCA. The Statistical Package for Social Science, IBM SPSS Statistics v20 [41] was used for all the statistical analysis. The Squared Euclidean Distance was chosen as the similarity/dissimilarity determinant to partition the data into their respective groupings and subsequently regrouped using the Ward's agglomeration method [42,43]. Determining the number of clusters in the HCA analysis is a semi-objective process and requires knowledge of the underlying geological, hydrogeological and prevailing environmental conditions [26,40]. The output of the number of clusters depends on the position of the critical linkage distance on the dendrogram. It is always a good practice to choose an appropriate linkage distance so as not to generate too many or too few groupings in order not to complicate interpretation or to omit certain important hydrochemical processes. In our case, a linkage distance of 3.5 was chosen and resulted in three clusters. The samples under each cluster and their positions were then plotted and used as the basis to understand the groundwater chemical evolution along the flow regime.

3. Results

Overall, the hydrochemical data of the surface water and groundwater samples show large variations across the entire dataset. During the field campaign, we found that most of the surface water samples were turbid with a brownish color mainly due to the impact of illegal mining. All wells sampled are public wells that are active and serve as the main water supply for the communities in the catchment area, however, the quality of the samples is not checked regularly. Information on the historical drill hole logs including the quality report and drill depths for some of the wells is not available. The hydrochemical data and details about the field and laboratory measurements can be found in Manu et al. [33].

3.1. Surface Water Chemistry

Figure 3a shows the variation in the major ions and trace metal composition of the surface water samples. As can be seen, the order of cation and anion abundance is $\text{Na}^+ > \text{Ca}^{2+} > \text{K}^+ > \text{Mg}^{2+}$ and $\text{HCO}_3^- > \text{Cl}^- > \text{SO}_4^{2-} > \text{NO}_3^-$, respectively. We have observed that the cations show relatively less variability than the anions. The largest variability in the hydrochemical data is associated with NO_3^- and SO_4^{2-} . The pH of surface water is generally mildly acidic to alkaline with a mean and standard deviation of 7.3 and ± 0.3 , respectively. The electrical conductivity ranges from 18 to 607 $\mu\text{S}/\text{cm}$ with a mean and standard deviation of 157 $\mu\text{S}/\text{cm}$ and ± 101 $\mu\text{S}/\text{cm}$, respectively. The temperature is less variable and ranges from 28 to 32 $^\circ\text{C}$ with a mean and standard deviation of 28.5 $^\circ\text{C}$ and ± 1.4 $^\circ\text{C}$, respectively. The dissolved oxygen (DO) ranges between 0.3 mg/L and 2.1 mg/L with a mean and a standard deviation of 1.5 mg/L and ± 0.5 mg/L, respectively. For trace metals, Fe (total) concentration was relatively higher than that of the Mn. The highest Fe (total) concentration occurs in the southern areas, while the northern areas have high Mn concentrations.

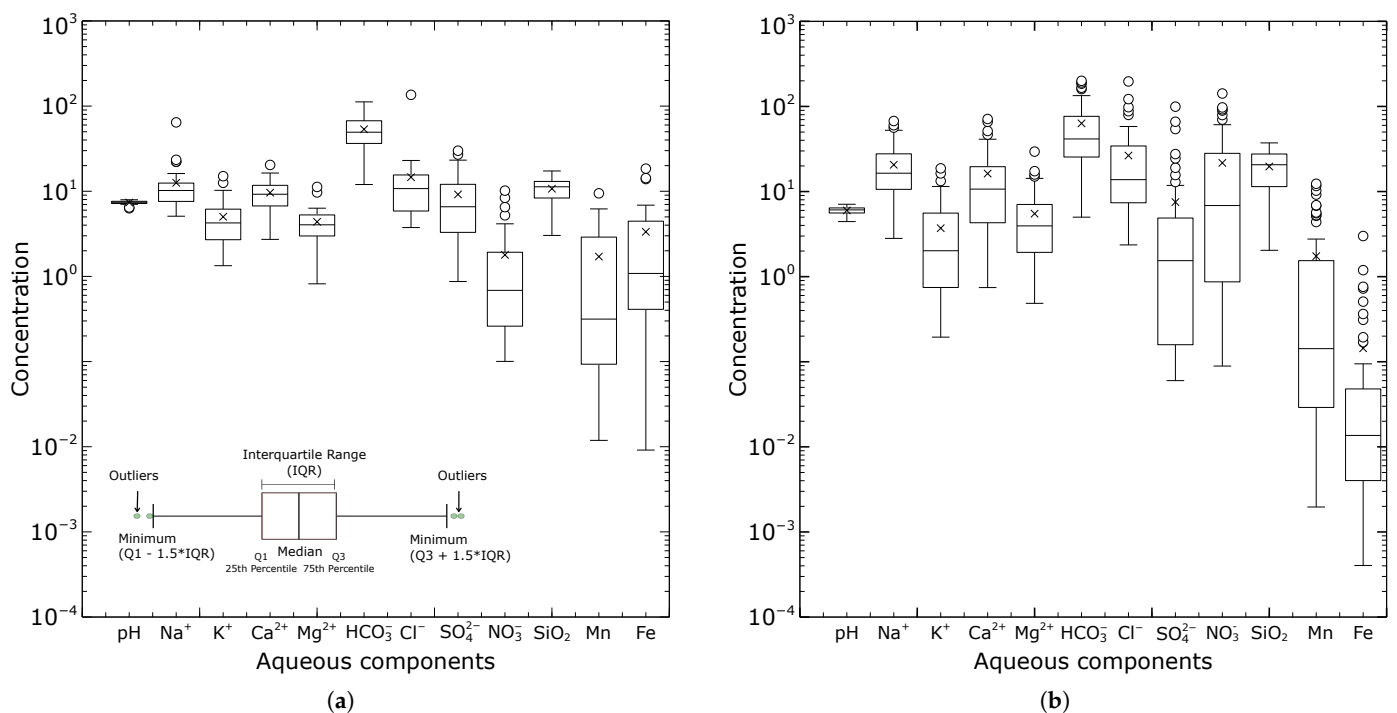


Figure 3. The box-and-whisker plots show the relative abundance of major ions, trace metals and silica in surface water (a) and groundwater (b). The horizontal solid line and the x symbol on the box-and-whisker plot represent the average and the median concentrations, respectively. Outliers are defined by points that fall more than 1.5*IQR above the third quartile or below the first quartile. All the ion concentrations are measured in mg/L except pH.

3.2. Groundwater Chemistry

Figure 3b shows the statistical summary of groundwater chemical composition. The pH of the groundwater is generally acidic to neutral and shows homogeneity in its data set. The order of cation abundance is $\text{Na}^+ > \text{Ca}^{2+} > \text{Mg}^{2+} > \text{K}^+$ while that of the anions is $\text{HCO}_3^- > \text{Cl}^- > \text{NO}_3^- > \text{SO}_4^{2-}$. Among the major ions, NO_3^- and SO_4^{2-} show the greatest variability in their concentrations. For the trace metals, the Mn concentration is relatively higher than that of Fe (total), with both parameters exhibiting large variations. We observed a significant number of the groundwater samples with measured Fe (total) concentrations below the detection limit. The dissolved oxygen ranges from 0.4 to 2.8 mg/L with a mean and standard deviation of 1.2 mg/L and ± 0.5 mg/L, respectively. As for the physical parameters, the temperature ranges from 27 to 31 °C with an average and standard deviation of 28.5 °C and ± 1.2 °C, respectively. The electrical conductivity ranges from 33 to 795 $\mu\text{S}/\text{cm}$ with a mean and standard deviation of 239.0 $\mu\text{S}/\text{cm}$ and ± 164 $\mu\text{S}/\text{cm}$, respectively. The highest EC values are associated with the samples in the southern areas, while the northern areas are characteristically low.

3.3. Calculation of Surface Water Quality Indices for Drinking and Irrigation

Figure 4a shows the spatial distribution of the calculated surface water quality index (WQI). As can be seen, 25 out of 34, representing 74% of the surface water samples, had $\text{WQI} > 100$ and are classified as poor to unsuitable for drinking. Surface water samples from the northern area are influenced by Mn, while Fe (total) influences samples in the central and southern areas. Our analyses show that all major ion concentrations are well within the WHO standard limits for drinking water. However, we find that the Fe (total) concentration in 27 out of 34 samples exceeds the WHO limit of 0.3 mg/L Fe (total) in drinking water, while the Mn concentration in 15 out of 35 samples exceeds the acceptable limit of 0.1 mg/L. The surface water quality is significantly influenced by the high Mn and Fe (total) contents in the surface water samples.

For irrigation purposes, the water quality indices SAR, USSL and the Wilcox diagram show good to excellent surface water quality. Figure 4b shows the spatial distribution of the calculated SAR, which is broadly within the acceptable limit of $\text{SAR} < 10$ for irrigation water. We see from Figure 5a that 32 out of 34 samples fall into the C1 S1 (low salinity, low sodicity) category of irrigation water. Only three samples fall into the C2 S1 category (medium salinity, low sodicity). Based on the Wilcox classification (Figure 5b), we find all surface water samples in the excellent to good irrigation water category.

3.4. Calculation of Groundwater Quality Indices for Drinking and Irrigation

Figure 6a shows the spatial distribution of the WQI used to assess the drinking water quality of the groundwater. As can be seen, a total of 44 out of 56 groundwater samples had a $\text{WQI} < 100$ and fall into the category of good to excellent drinking water. However, twelve samples showed a $\text{WQI} > 100$ and fall into the poor to unsuitable category. Eleven of the samples classified as poor to unsuitable are located in the northern areas of the basin. We find that all major ion concentrations including Na^+ , K^+ , Ca^{2+} , Mg^{2+} , Cl^- , HCO_3^- , SO_4^{2-} and NO_3^- are well within the limits of the WHO drinking water guidelines [35], with the exception of eight samples where NO_3^- exceeded the acceptable limit of 50 mg/L nitrate in drinking water. For trace metals, the Fe (total) concentration in most groundwater samples (50 out of 56) is within the WHO acceptable drinking limit of 0.3 mg/L, while 6 samples were above it. The Mn concentration in twenty samples exceeded the WHO value of 0.4 mg/L Mn in drinking water. All samples with the high Mn concentration are located in the northern parts of the basin.

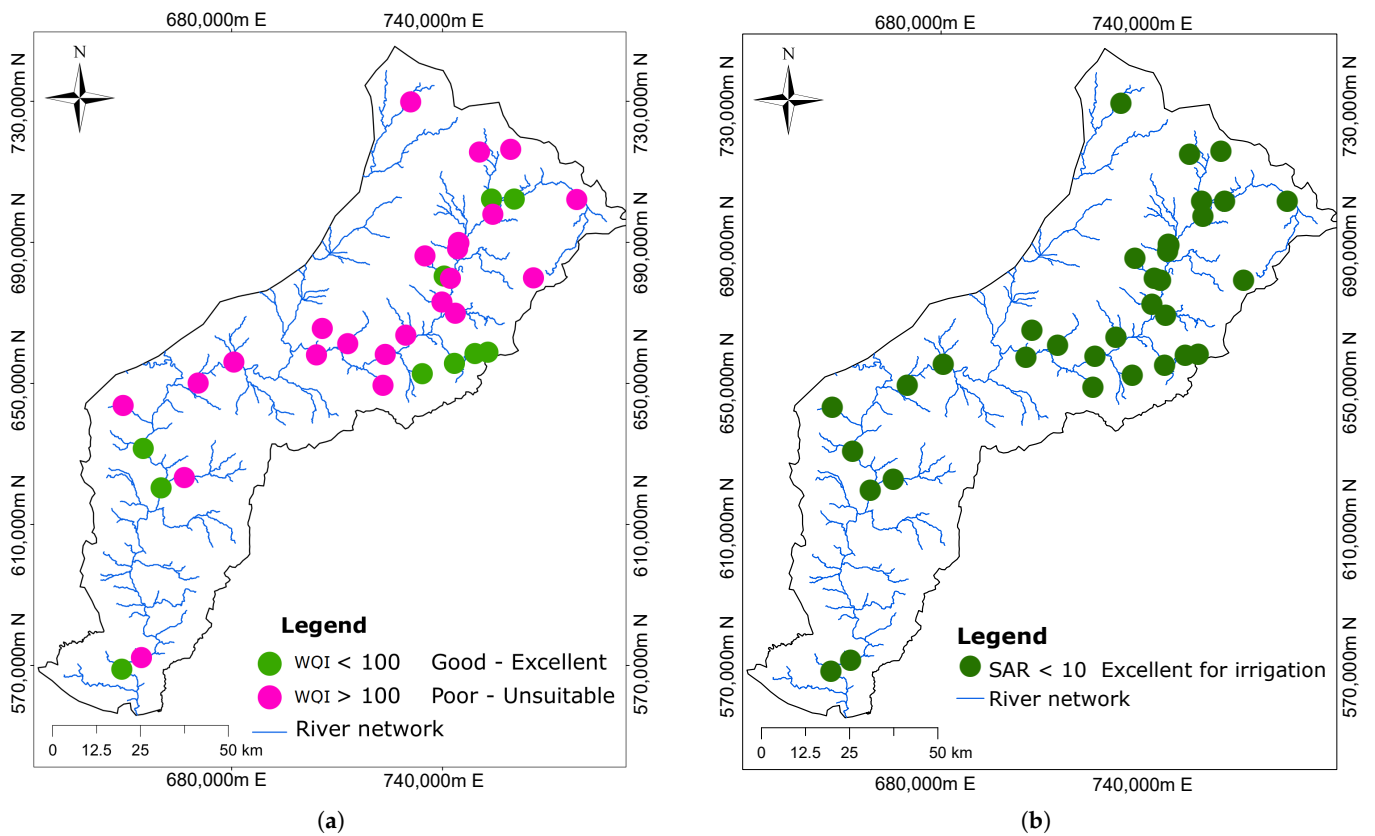


Figure 4. Surface water spatial distribution maps of (a) Water Quality Index (WQI) and (b) Sodium Adsorption Ratio (SAR) for the assessment of water quality for drinking and irrigation purposes

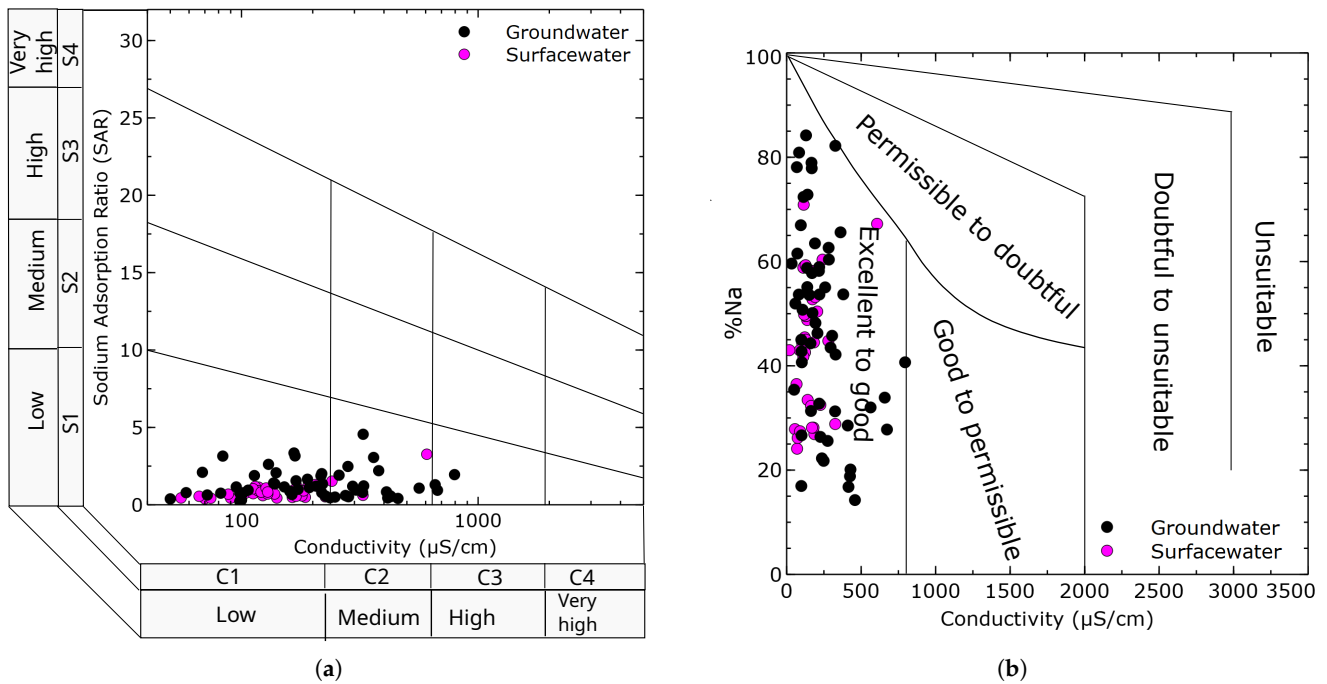


Figure 5. Irrigation water classification diagrams showing surface water and groundwater quality acceptable for irrigation (a) USSL classification [36] and (b) Wilcox classification [44].

For irrigation quality assesment, the SAR, USSL and Wilcox diagram show that all groundwater samples fall into the good to excellent irrigation water category. The spatial

distribution of the calculated SAR is shown in Figure 6b. We see that all groundwater samples have a SAR > 10 and above in the good to excellent irrigation water category. Figure 5a shows the distribution of the samples in the USSL diagram. Almost all the groundwater samples are within the the C1 S1 (low salinity—low sodicity) and C2 S2 (medium salinity—low sodicity) categories of irrigation water. Three samples plot within the C3 S1 area representing a high salinity—low sodicity water. Figure 5b shows the distribution of the groundwater samples on the Wilcox plot and highlights that all the samples fall in the category of excellent to good quality irrigation water with an electrical conductivity less than 1000 $\mu\text{S}/\text{cm}$.

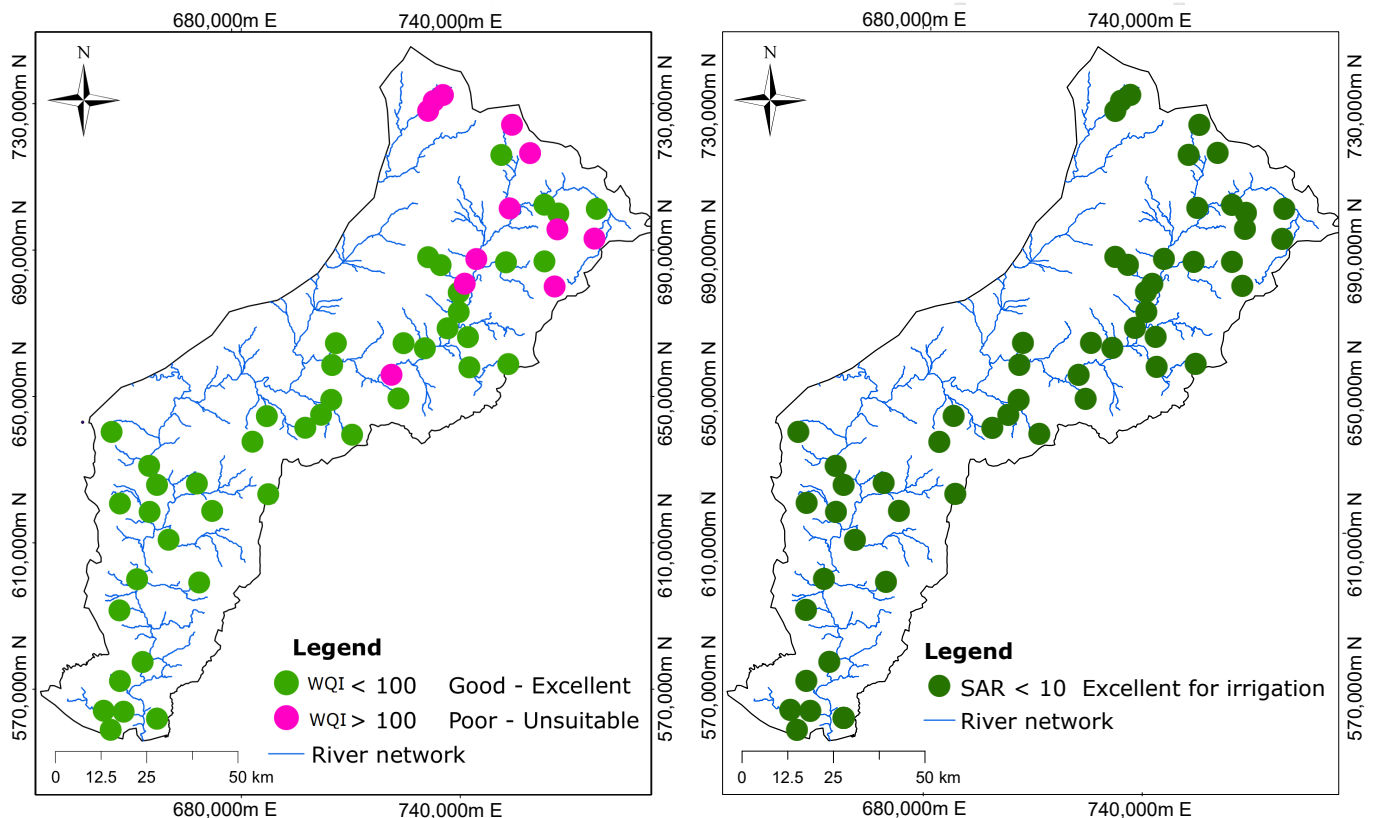


Figure 6. Groundwater spatial distribution maps of (a) Water Quality Index (WQI) and (b) Sodium Adsorption Ratio (SAR) for the assessment of water quality for drinking and irrigation purposes.

3.5. Hierarchical Cluster Analysis (HCA) of the Groundwater Hydrochemical Data

HCA performed on the groundwater chemical data revealed three clusters that do not show a clear pattern (Figure 7A), underscoring that the hydrochemical environment is heterogeneous at the basin scale. Here we see that the water compositions are variable across the two major lithologies. The spatial association in hydrochemistry is not identifiable based on the underlying geology.

However, HCA provides three distinct spatial associations, taking into account elevation (Figure 7B), consistent with general groundwater flow under the influence of topography. Based on elevation, we see that the northern zone samples are at higher elevations, the central zone is at intermediate, and the southern zone is at lower elevations. These three zonations were defined to facilitate the interpretation of the hydrochemical dataset, which is variable at the basin scale.

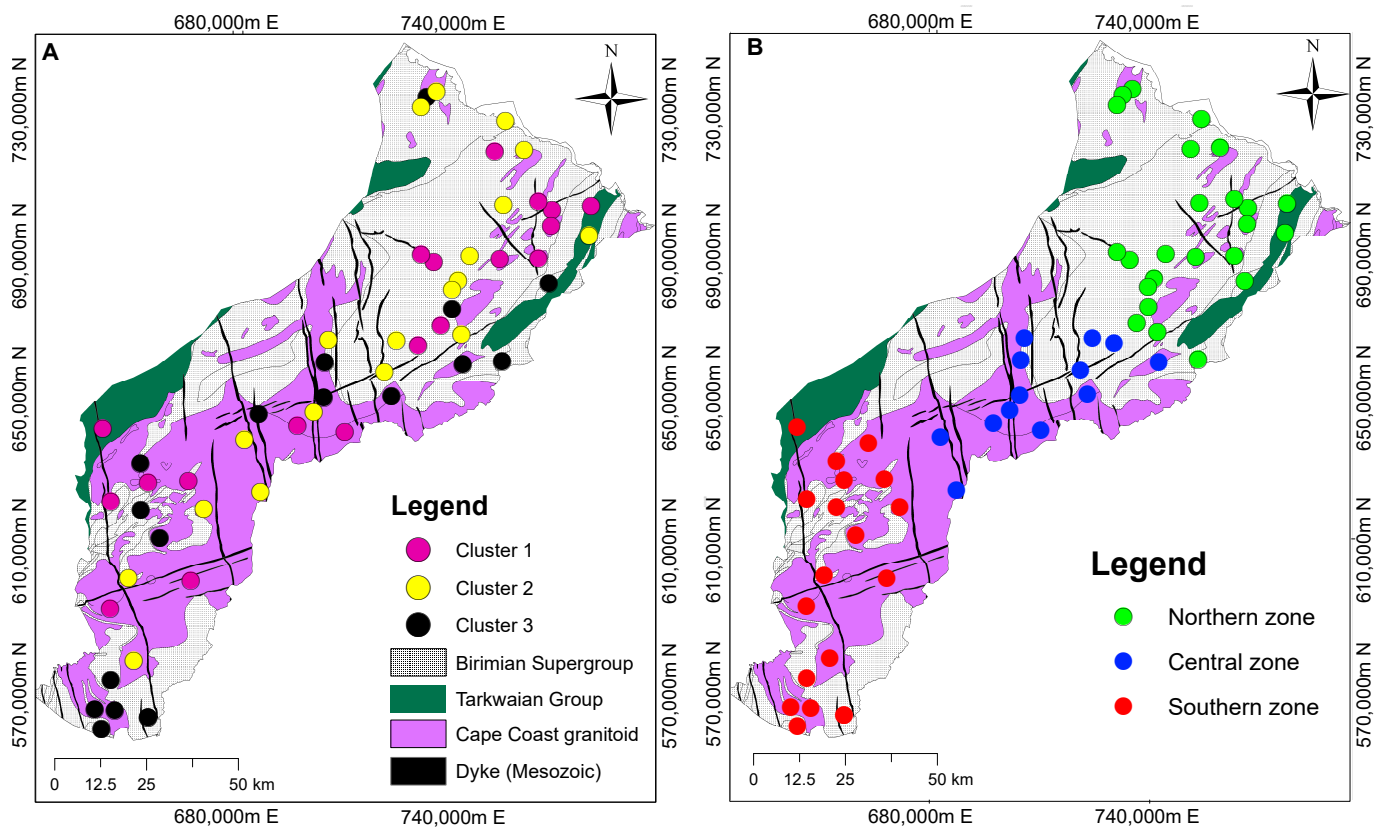


Figure 7. Hierarchical cluster analysis (HCA) of the hydrochemical dataset. (A) Taking into account only hydrochemical data, three clusters are identified with no apparent geographical proximity, highlighting large variability across the basin. (B) Considering elevation for the HCA, three spatially distinct clusters appear, dividing the basin into three zones: northern, central and southern. The elevation is highest in the northern zone and decreases towards the southern zone.

3.6. Groundwater Chemical Variation within the Three Defined Zones

Groundwater chemistry exhibits large variability in chemical composition, with the largest variability observed in samples from the southern zone of the area. Figure 8a,b shows the box-and-whisker plot of the physical and chemical parameters in the groundwater for the three zones, respectively. The northern zone has the widest spread and variability in pH with an estimated standard deviation of ± 0.74 . The southern zone recorded the highest variability in the electrical conductivity with an estimated standard deviation of $\pm 196 \mu\text{S}/\text{cm}$. From Figure 8a, the groundwater of the northern and southern zones has the widest spread in dissolved oxygen (DO) and exhibits mixed reducing conditions. The central zone has the lowest deviation in DO and exhibits oxic conditions in most groundwater samples.

Our results indicate that Na^+ , Ca^{2+} and HCO_3^- are the abundant ions in groundwater. The order of cation occurrence in the northern zone is $\text{Ca}^{2+} > \text{Na}^+ > \text{Mg}^{2+} > \text{K}^+$, the central zone is $\text{Na}^+ > \text{Ca}^{2+} > \text{Mg}^{2+} > \text{K}^+$ and the southern zone is $\text{Na}^+ > \text{Ca}^{2+} > \text{Mg}^{2+} > \text{K}^+$ (Figure 8b). For anions (Figure 9), the order of abundance is $\text{HCO}_3^- > \text{NO}_3^- > \text{Cl}^- > \text{SO}_4^{2-}$ (northern zone), $\text{HCO}_3^- > \text{Cl}^- > \text{NO}_3^- > \text{SO}_4^{2-}$ (central zone) and $\text{Cl}^- > \text{HCO}_3^- > \text{NO}_3^- > \text{SO}_4^{2-}$ (southern zone). In the northern zone, Ca^{2+} and Na^+ account for about 80% of the total cation concentrations, while HCO_3^- accounts for 65% of the total anion concentrations. In the central zone, Ca^{2+} and Na^+ contribute about 80% of the total cations, with HCO_3^- and Cl^- account for 57% and 24% of the total anions. In the southern zone, Na^+ contributes about 50% while Ca^{2+} accounts for 30% of the cations. Anions in the southern zone consist of 37% HCO_3^- , 32% Cl^- and 20% NO_3^- . All three zones show very low concentrations of K^+ and SO_4^{2-} .

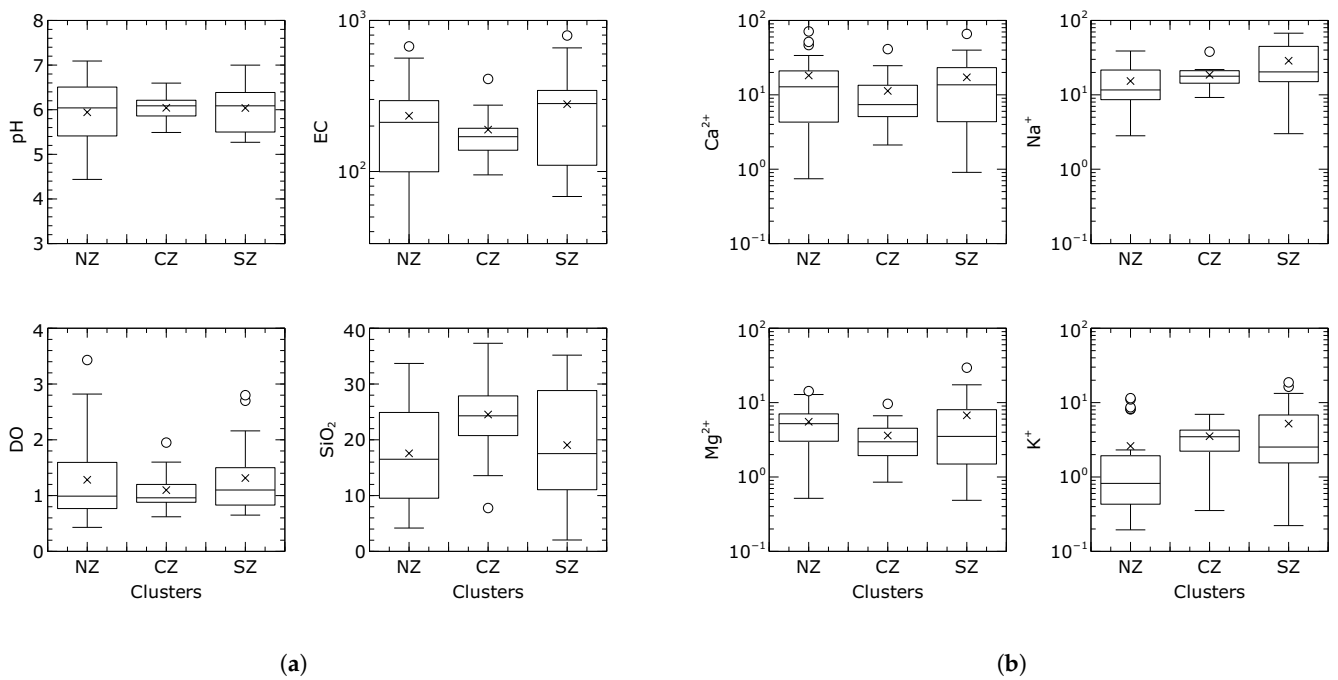


Figure 8. Box-and-whisker plots displaying the variations in the (a) physical parameters and silica content, and (b) major cations in the groundwater. The interpretation of the box-and-whisker plots follows the legend presented in Figure 3. The horizontal solid line and the x symbol on the box-and-whisker plot represents the average and the median concentrations, respectively. Outliers are defined by points that fall more than 1.5*IQR above the third quartile or below the first quartile. NZ, CZ and SZ denote the northern zone, central zone and southern zone, respectively. All chemical parameters are measured in mg/L except for pH and EC µS/cm.

Table 2 shows the results of selected correlation coefficients between the hydrochemical parameters in the groundwater and highlights relationships between them. They were tested at a significance level of $p < 0.05$ with $r > 0.7$ and $r < 0.5$ indicating strong and weak correlations [27,45], respectively. In the northern zone groundwater samples, there is a strong positive correlation between pH and HCO₃⁻, EC and Ca²⁺, EC and HCO₃⁻, Ca²⁺ and HCO₃⁻ and Na⁺ and Cl⁻. In the central zone, there is a strong correlation between pH and SiO₄, pH and Ca²⁺, EC and Ca²⁺, Ca²⁺ and Cl⁻, and Na⁺ and Mg²⁺. The southern zone also shows a strong positive correlation between pH and HCO₃⁻, EC and Ca²⁺, EC and Na⁺, EC and Cl⁻, Ca²⁺ and Cl⁻ and Na⁺ and Cl⁻. These correlations show that several factors combine in the evolution of hydrochemical parameters in the groundwater and provide a potential source for them. Within these relationships, Ca²⁺, Na⁺, Cl⁻ and HCO₃⁻ contribute significantly to the EC in groundwater.

Table 2. Correlation coefficients between the hydrochemical parameters in the groundwater, highlighting the relationships between them. They were tested at a significance level of $p < 0.05$ with $r > 0.7$ and $r < 0.5$ indicating stronger and weaker correlations [27,45], respectively. Only the correlations with r-values > 0.7 are considered significant and presented here.

Zone	pH-HCO ₃ ⁻	pH-SiO ₄	pH-Ca ²⁺	EC-Ca ²⁺	EC-Na ⁺	EC-Cl ⁻	EC-HCO ₃ ⁻	Ca ²⁺ -HCO ₃ ⁻	Ca ²⁺ -Cl ⁻	Na ⁺ -Cl ⁻	Na ⁺ -Mg ²⁺
Northern	0.70	-	-	0.93	-	-	0.87	0.87	-	0.88	-
Central	-	0.80	0.75	0.96	-	-	-	-	0.76	-	0.73
Southern	0.79	-	-	0.92	0.72	0.88	-	-	0.76	0.84	-

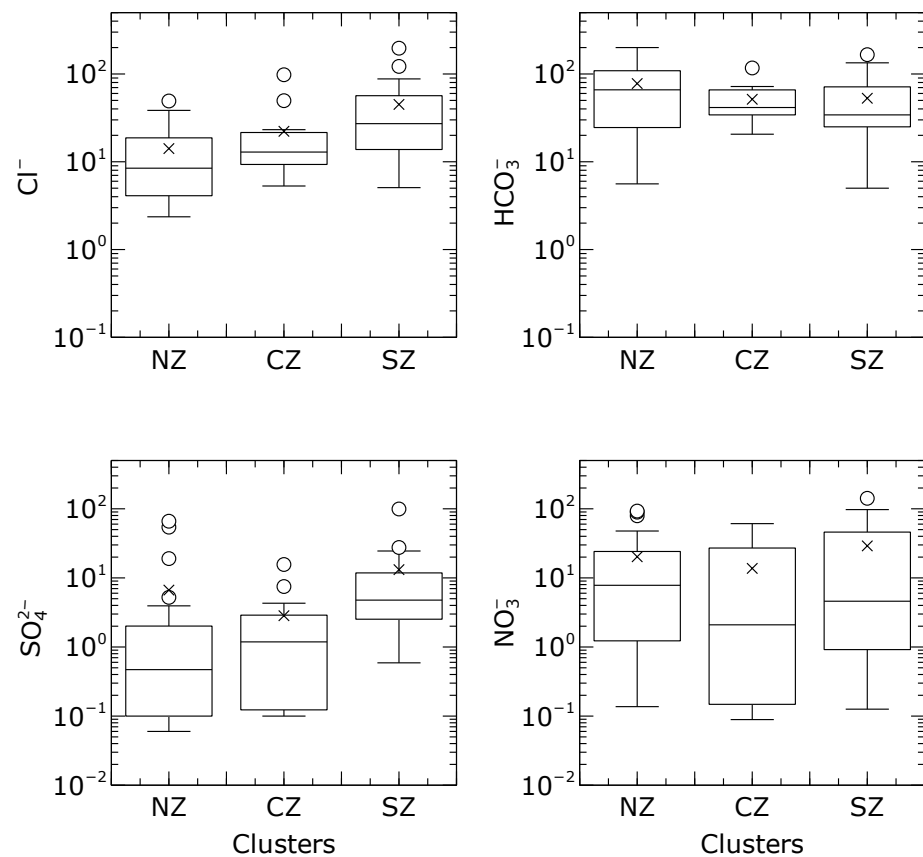


Figure 9. Box- and-whisker plots highlighting the variations in the major anions (HCO_3^- , Cl^- , SO_4^{2-} and NO_3^-) in groundwater for the three identified zones. The horizontal solid line and the x symbol on the box-and-whisker plot represents the average and the median concentrations, respectively. Outliers are defined by points that fall more than $1.5 \times \text{IQR}$ above the third quartile or below the first quartile. NZ, CZ and SZ denote the northern zone, central zone and southern zone, respectively. All chemical parameters are measured in mg/L.

3.7. Groundwater Types

The hydrochemical plot using the trilinear Piper diagram [46] shows variable water composition throughout the study area. A qualitative examination of the Piper diagram (Figure 10) shows that the samples from the southern zone are the most widespread and have the most diverse water composition. In the northern zone, 21 out of 25 samples are of Ca-HCO₃ water type, while 4 samples have mixed water compositions. Looking at the central zone, 8 out of 13 samples show a mixed water type dominated by Na-HCO₃. The southern zone exhibits a Na-Cl-dominant composition.

We observe from Figure 10 that in the northern zone, the alkaline earth metals (Ca^{2+} and Mg^{2+}) exceed the alkalis (Na^+ and K^+) while in the central zone the alkalis dominate the alkaline earth metals. The southern zone shows the dominance of the alkalis over the alkaline earth metals.

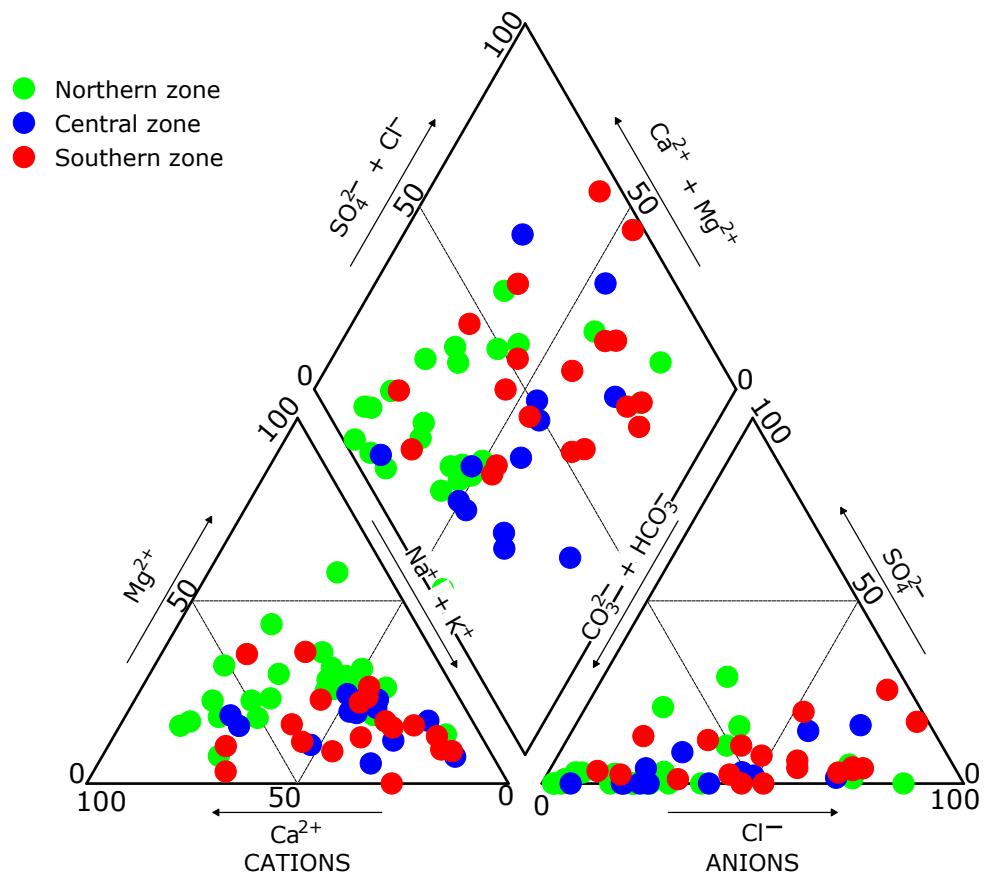


Figure 10. Piper diagram presenting the dominant ion species in the groundwater.

3.8. Mineral Weathering Processes

Figure 11 shows the results from the Gibbs diagram and underlines that the interaction between water and rock is the main mechanism driving the hydrochemistry in the study area. The plot of $\text{Na}^+ / (\text{Ca}^{2+} + \text{Na}^+)$ and $\text{Cl}^- / (\text{Cl}^- + \text{HCO}_3^-)$ ratios expressed as meq/L vs. TDS (mg/L) show that most of the samples plot in the rock dominance region, indicating the anion and cation composition of groundwater is derived from weathering processes.

We observe that the groundwater chemistry is driven by a higher $\text{Na}^+ / (\text{Ca}^{2+} + \text{Na}^+)$ ratio as a significant number of the points fall on the right side of the plot. The points distribution in the $\text{Cl}^- / (\text{Cl}^- + \text{HCO}_3^-)$ vs. TDS shows an increase in Cl^- relative to HCO_3^- along the flow regime from the north to the south of the basin.

Figure 12 shows the binary ion plots of the hydrochemical data and highlights the potential geochemical processes driving groundwater chemistry, including silicate weathering and cation exchange processes. The Na^+ vs. Cl^- plot (Figure 12a) shows that 19 of 24 samples from the northern zone, all 13 samples from the central zone and 14 of 19 samples from the southern zone plot in the silicate mineral weathering area. From the chloro-alkaline indices plot (Figure 12b), we found that almost all the groundwater samples except seven have negative chloro-alkaline indices values, which are dominantly distributed in the ion exchange area. We observed that one sample from the northern and four from the southern zone are plotted in the reverse ion exchange region. The HCO_3^- vs. Ca^{2+} plot (Figure 12c) shows the majority of the samples below the 1:1 line, emphasizing the excess of HCO_3^- over Ca^{2+} .

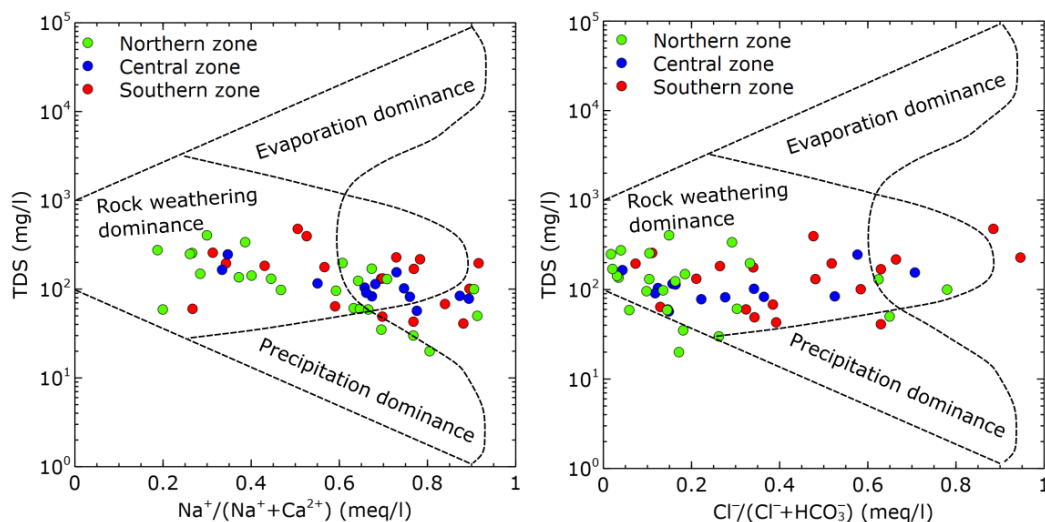


Figure 11. Gibbs diagram [47] for groundwater samples used to determine the main controls of water chemistry highlight rock weathering as the main mechanism controlling groundwater chemistry in the Pra Basin.

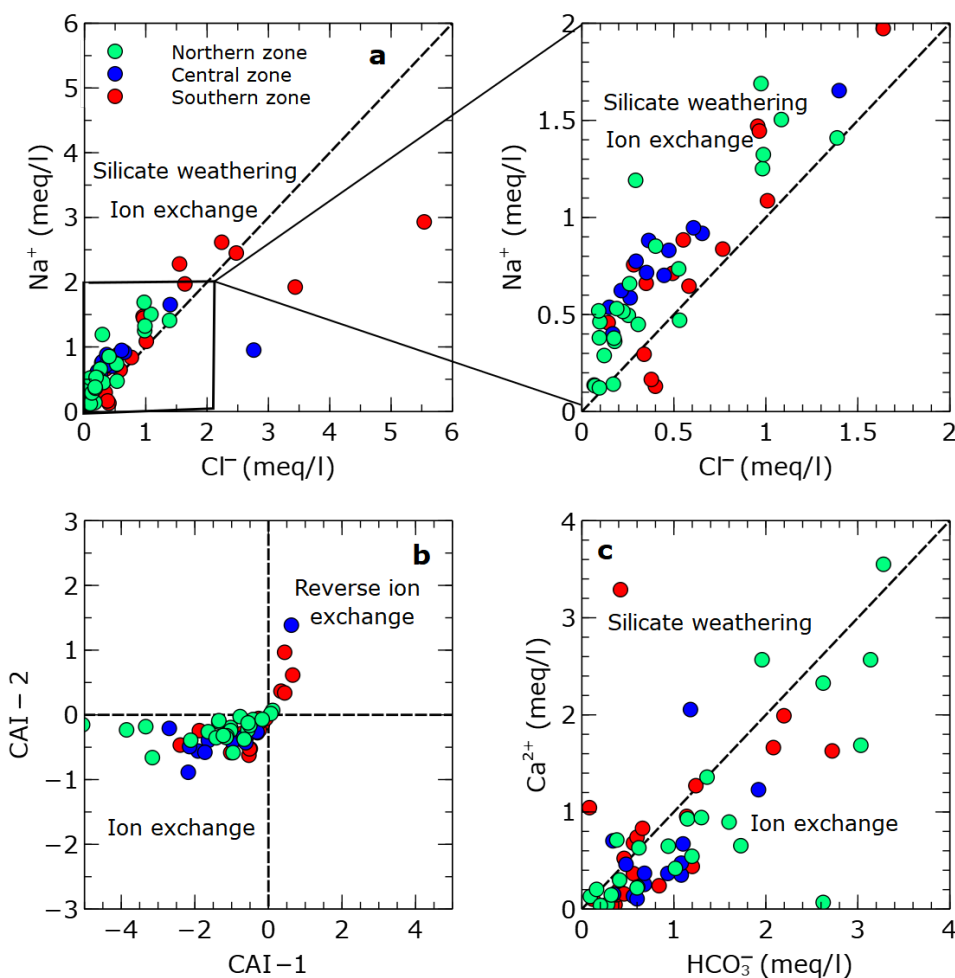


Figure 12. Bi-variate ion plots showing the most probable geochemical processes, including silicate weathering (a), and ion exchange (b,c) in the groundwater system.

3.9. Factor Analysis

Four factor models were generated, including each of the three zones (northern, central and southern) and the combined dataset with factor scores showing significant correlations explaining the variation in the groundwater chemical composition. In the northern zone, two factors accounted for 78% of the total variation in the dataset as presented in Table 3. Factor 1 explained 40% of the variance and loaded positively with pH, Ca²⁺, HCO₃⁻ and SiO₄, while Factor 2 loaded significantly with Na⁺, Cl⁻ and SO₄²⁻ and explained about 37% of the total variation (Table 3). Here, Ca²⁺, HCO₃⁻ and pH have the highest factor scores and thus have the relatively strongest influence among other parameters.

Table 3. Scores generated from the factor analysis explaining significant relationships between the hydrochemical parameters. The dash symbols (-) indicate that the parameter loaded a communality less than 0.5 and was deemed statistically insignificant and thus was not considered for the factor analysis.

Northern Zone (n = 24)	pH	Na ⁺	K ⁺	Ca ²⁺	Mg ²⁺	HCO ₃ ⁻	Cl ⁻	SO ₄ ²⁻	SiO ₄	% of Variance	Cumulative %
Fact 1	0.958	0.155	0.006	0.845	-	0.904	0.051	0.427	0.776	40.773	40.773
Fact 2	0.011	0.901	0.799	0.453	-	-0.021	0.938	0.666	0.189	37.702	78.475
Central Zone (n = 13)	pH	Na ⁺	K ⁺	Ca ²⁺	Mg ²⁺	HCO ₃ ⁻	Cl ⁻	SO ₄ ²⁻	SiO ₄	% of Variance	Cumulative %
Fact 1	0.922	-0.126	-0.009	0.719	0.188	0.767	0.025	-0.336	0.897	34.773	34.773
Fact 2	-0.247	0.839	0.166	0.575	0.818	-0.285	0.874	0.711	-0.043	33.589	68.362
Fact 3	0.052	0.36	0.952	-0.318	-0.318	-0.453	0.226	0.423	0.226	17.518	85.880
Southern Zone (n = 19)	pH	Na ⁺	K ⁺	Ca ²⁺	Mg ²⁺	HCO ₃ ⁻	Cl ⁻	SO ₄ ²⁻	SiO ₄	% of Variance	Cumulative %
Fact 1	-0.13	0.899	0.785	-	0.896	0.033	0.926	0.760	-	52.57	52.57
Fact 2	0.947	-0.048	0.248	-	0.231	0.932	-0.116	0.120	-	27.30	79.87
Combined (n = 56)	pH	Na ⁺	K ⁺	Ca ²⁺	Mg ²⁺	HCO ₃ ⁻	Cl ⁻	SO ₄ ²⁻	SiO ₄	% of Variance	Cumulative %
Fact 1	-0.060	0.898	0.789	0.445	-	-0.164	0.932	0.770	0.294	40.043	40.043
Fact 2	0.927	0.141	0.084	0.805	-	0.902	0.018	0.185	0.710	36.054	76.097

The central zone produced three factor scores, explaining about 86% of the variance in the hydrochemical data. The extracted factor model is presented in Table 3. Out of this Factor 1 and Factor 2 explained 35% and 34% of the variation, while Factor 3 explained 17% of the variation (Table 3). There is no clear identification of dominant process(es) influencing groundwater chemistry in the central zone.

In the southern zone, two factors scores explained approximately 80% of the total variance in the hydrochemistry (Table 3). Factor 1 explained about 53% of the total variance and was positively loaded with Na⁺, K⁺, Mg²⁺, Cl⁻ and SO₄²⁻, with Na⁺ and Cl⁻ providing the highest factor scores (Table 3). Factor 2 explained 27% and loaded positively with pH and HCO₃⁻.

Between the individual factor models, the northern zone is characterized by the dominance of Ca²⁺, HCO₃⁻ and pH, the southern zone is dominated by Na⁺ and Cl⁻ according to the factor scores. There is no dominant factor to explain the hydrochemical variation in the central zone. The central zone showed no dominance of ionic species and presented the highest number of factor models highlighting the influence of different processes on the hydrochemistry.

The factor analysis performed on the combined dataset resulted in two factor models accounting for 76% of the total variance in the hydrochemical dataset. Factor 1 loaded positively with Na⁺, K⁺, Cl⁻ and SO₄²⁻ (Table 3) and explained 40% of the variation. Factor 2 explained 36% of the variance and loaded positively with pH, Ca²⁺, HCO₃⁻ and S⁴⁺. The correlations between the parameters indicate different processes that control the hydrochemistry of the groundwater. The factor model of the combined data set presented the lowest cumulative percentage of variation and brings to bare the heterogeneity in the basin scale data set.

4. Discussion

4.1. Sampling and Measurements

A total of 90 water samples from surface water ($n = 34$) and groundwater ($n = 56$) were successfully analyzed for their chemical parameters. This is the first time such a comprehensive regional-scale hydrochemical study has been conducted in the Pra Basin before and after the ban on illegal mining activities. In general, common practice assumes that the cations and anions, which are the main chemical constituents in groundwater, must fall within the range of at least $\pm 5\%$ of each other [48,49]. In this study, the charge balance error (CBE) performed on the chemical data showed that most of the samples fell below $\pm 3\%$, reflecting good data quality. On the basis of the internal consistency check, the presented hydrochemical data of the surface water and groundwater is considered representative of the field conditions and thus can be used for further analysis.

4.2. Assessment of Surface Water Quality for Drinking and Irrigation

The surface water in the Pra Basin is of poor quality for drinking, supposedly due to the illegal mining activities in the area. Our analysis shows that Mn and Fe (total) are the two pollutants affecting surface water quality. To our knowledge, the high concentrations of Mn and Fe (total) might be facilitated by illegal mining involving underground excavation, digging and washing in the rivers in search of mineral resources. In the study area, the saprolite and the duricrust overlying the bedrock contain minerals of pyrite, iron oxides and Mn-rich sediments [50]. When exposed to water, these minerals dissolve, releasing Mn and Fe (total) into the water and increasing their concentration in surface water.

Our results agree broadly with the results of Bessah et al. [51] who studied the surface water quality of the Pra Basin. In their study, the authors sampled surface water from 25 rivers in the Pra Basin and showed that 80% of the samples had Fe (total) concentrations above the WHO standard in drinking water. They found high concentrations of Cu, Hg, As and Fe (total), above the acceptable levels for drinking water. The presence of mercury in the surface waters of the Pra Basin has been attributed to illegal mining activities where the use of mercury to extract gold is common. Darko et al. [52] also reported turbidity in some nearby rivers ranging from 12 to 4645 NTU, which is above the acceptable limits of 5 NTU in surface water bodies [52]. Their study also found Fe (total) concentrations as high as 30 mg/L with a mean of 7.7 mg/L, above the WHO standard of 0.1 mg/L for drinking water. The high turbidity and excessive levels of Fe (total) and Hg in the surface water are likely caused by the illegal mining activities pervasive in the Pra Basin.

Irrigation quality indices such as SAR, USSL and the Wilcox diagram classify the surface water as suitable for irrigation. The calculated indices for irrigation were based on the ions including Na^+ , K^+ , Ca^{2+} and Mg^{2+} as these are known to have negative effects on soil and also on plants when present in excess. We observed very low levels of Na^+ , which is good for soil maintenance. Excess sodium in the water affects the hydraulic conductivity of the soil and is an important factor when considering water for irrigation. Generally, water with a SAR < 10 is considered excellent for irrigation [37]. Based on this criterion, the surface waters can be interpreted as suitable for irrigation. This is confirmed by the USSL and Wilcox plots based on the sodium and electrical conductivity of the water.

Regarding the trace metals (Fe (total) and Mn), our results indicate that surface water may require some treatment before being used for irrigation. In general, irrigation water with Fe (total) and Mn concentrations less than 5 mg/L and 0.2 mg/L [53], respectively, is considered acceptable for irrigation. Excessive levels of these trace metals have been reported as a possible cause of clogging and rusting of irrigation systems [54]. In general, Fe is not toxic to plants. However, extreme levels can lead to soil acidification and depletion of essential plant nutrients such as phosphorus and molybdenum [53,54]. Manganese, on the other hand, is toxic to some plants in acid soils [53], and its presence must be controlled depending on the type of plants to be irrigated. In this study, 24% of Fe (total) and 47% of Mn concentrations in surface water are above their respective limits in irrigation water and, therefore may require treatment to reduce concentrations to acceptable levels before use.

4.3. Assessment of Groundwater Quality for Drinking and Irrigation

Our analysis shows that groundwater quality in the central and southern zones is excellent for drinking, while the northern zone is of poor quality, affected by Mn and Fe. Samples from the central and southern zones are largely from the Cape Coast granitoid aquifers. The granitoid generally consists of silicates. Due to the slow rate of weathering of silicate minerals, the amount of dissolved ions is very low and within WHO guidelines for drinking water. All major ionic concentrations are within the desirable limits of WHO guideline levels in drinking water. In our analysis, we find that without including trace metals, such as Fe (total) and Mn, in the WQI calculations, all samples fall in the good to excellent category, consistent with a comparison based on WHO guideline values for each major ion. However, considering Mn and Fe (total) in the WQI analysis, we find that 13 samples, all located in the northern zone, are of poor quality and cannot be used for drinking. To the best of our knowledge, the sources of Mn and Fe (total) are likely from the rock and leaching from polluted surface waters. The rocks beneath the northern zone are mostly meta-sediments containing pyrite, iron oxides and Mn-rich minerals [50]. As water interacts with the rocks in the aquifer, more ions, including Mn and Fe (total), are released into the solution. On the other hand, due to the high Mn and Fe (total) contents in surface waters, it is also likely that they were transported from the surface into the aquifer in areas where the hydraulic connection between groundwater and surface water exists.

Our analysis based on the SAR, USSL and the Wilcox irrigation schemes show that groundwater is of excellent quality for irrigation. In general, crystalline bedrock aquifers produce excellent water quality for crop irrigation [21,55–60]. The quality of the water used for irrigation depends on the concentration of ions leaching into the groundwater from the underlying geological material. Such ions include Na^+ , K^+ , Ca^{2+} , Mg^{2+} , HCO_3^- , Cl^- , SO_4^{2-} and NO_3^- . In this study, the major ion concentrations of the groundwater is generally low and this can be attributed to the slow weathering of the crystalline rocks.

With regard to trace metals (Mn and Fe (total)), the groundwater of the northern zone has relatively higher concentrations of Mn and Fe (total) than those of the central and southern zones. In view of this, water extracted from the northern zone aquifers may require some treatment prior to use. However, the groundwater in the central and southern zones could be used without treatment.

4.4. Mechanism Controlling Groundwater Chemistry

Theoretically, three mechanisms controlling the dissolved ions in groundwater can be derived from the Gibbs diagram, depending on rock dominance, precipitation dominance and evaporation dominance. It is evident that most groundwater samples are plotted in the rock-dominance region (Figure 11), suggesting that rock weathering is an important mechanism controlling groundwater chemistry in the study area. According to Banks and Frengstad [61], the ratio of $\text{Na}^+ / (\text{Na}^+ + \text{Ca}^{2+})$ in silicate-dominated environments can exceed 0.9, which is the maximum limit in the Gibbs diagram. In such cases, the groundwater chemistry is driven by a high $\text{Na}^+ / (\text{Na}^+ + \text{Ca}^{2+})$ ratio and the points on the Gibbs diagram shifts to the right outside of the boomerang. Our results support this hypothesis, as some of our groundwater samples show a $\text{Na}^+ / (\text{Na}^+ + \text{Ca}^{2+})$ ratio greater than 0.9, underscoring that silicate weathering is an important process driving groundwater chemistry in the area, consistent with several studies that identified the weathering of silicates as a dominant geochemical process in similar rock environments [15,19,58].

4.5. Chemical Processes Driving Groundwater Evolution

Bivariate ion plots in Figure 12 show that groundwater chemistry is mainly controlled by silicate weathering, carbonate dissolution and ion exchange reactions. From Figure 12a we see that there is an excess of Na^+ relative to Cl^- , indicating an additional source of the Na^+ in the solution. Meybeck [62] reported that a $\text{Na}^+ / \text{Cl}^-$ ratio greater than 1 emphasises silicate weathering as a source of Na^+ . Again, the excess Na^+ in the solution likely comes from ion exchange where the Ca^{2+} in the solution is exchanged for Na^+ from the aquifer

matrix. Freeze and Cherry [63] and Appelo and Postma [49] underscored that that if Na^+ is released mainly by silicate weathering, HCO_3^- will be the most abundant anion in groundwater, which is generally the case in the northern and central zones, however in the southern zone Cl^- is the most dominant anion interpreted to originate from the dissolution of marine aerosols from the sea.

From Figure 12b,c, we learn that ion exchange and carbonate dissolution do occur in the groundwater system of the Pra Basin. Schoeller [38] proposed two indices which are used to determine the occurrence of ion exchange in a natural water system. He observed that when ion exchange occurs, the indices will be negative, indicating Na^+ - Ca^{2+} ion exchange, and when positive, indicate the reverse. Based on the Chloro-Alkaline Indices plot, we found that the majority of the samples show a negative value, indicating a Na^+ - Ca^{2+} exchange. Here Na^+ in the aquifer matrix exchanges with Ca^{2+} in solution, leading to a depletion of Ca^{2+} . A similar trend was observed in the Ca^{2+} vs. HCO_3^- plot as most samples are plotted on the HCO_3^- side. These two plots show that Ca^{2+} is exchanged with Na^+ in our groundwater system, suggesting that cation exchange affects the chemical composition of groundwater in the area. In addition to ion exchange, the points plotted along the 1:1 line in Figure 12c indicate a common source for Ca^{2+} and HCO_3^- that can be attributed to carbonate dissolution. The influence of carbonate dissolution plays a role in the hydrochemical evolution of the groundwater in the northern and central zones of the basin where calcite is found in the rocks [50].

4.6. Statistical Analysis Explaining the Causes of Spatial Variability in Groundwater Composition

Our analysis based on the HCA shows that hydrochemical variation in groundwater is determined by elevation, while factor scores revealed silicate weathering and carbonate dissolution as the plausible geochemical processes driving groundwater chemistry in the Pra Basin. Three spatially distinct chemical associations were identified from the HCA based on sample locations at either higher, intermediate, or lower elevations. Under natural conditions, groundwater is expected to flow from higher to lower elevations. For this reason, the higher elevation (northern zone) and the lower elevation (southern zone) are interpreted as recharge and discharge zones, respectively. The central zone, marked by an intermediate elevation, is interpreted as a transition zone along the flow path. From this, the groundwater in the study area is most likely to flow in the direction from the northern zone through the central and finally to the southern zone.

Chemically, the groundwater composition in the three defined zones changes from Ca- HCO_3 to a mixed water type dominated by Na- HCO_3 and a dominant Na-Cl water along the flow regime from the recharge to the discharge zone, respectively. In principle, the chemical composition of groundwater in the recharge zone is dominated by Ca- HCO_3 , which represents waters that have not interacted much with the rocks and are only in the early stages of evolution [58,64]. The prevalence of HCO_3^- in the northern zone is partially influenced by the CO_2 of the soil zone and the highly CO_2 -charged rainwater. Here the dominance of the Ca^{2+} could be attributed to the dissolution of carbonate, which is identified in the Birimian rocks underlying the northern zone [33,50]. The latter probably contributes to the HCO_3^- in the water composition of the northern zone. Factor analysis performed on the northern zone water samples revealed two factors, with Factor 1 explaining 40% of the overall variance in hydrochemistry. Factor 1 shows a positive correlation for pH, Ca^{2+} , HCO_3^- and SiO_2 , which we interpret as a consequence of silicate weathering and carbonate dissolution. This is consistent with the general mineralogical composition of the rocks in the area which have been found to contain silicates (albite, K-feldspar, muscovite and biotite) and carbonate minerals (calcite) [50,65]. The high positive correlation between Ca^{2+} and HCO_3^- indicates the dominance of these ions in groundwater and confirms the Ca- HCO_3 water type preserved in the northern zone.

In the transition zone, which is characterised by intermediate elevations, the chemical composition of the groundwater changes from the Ca- HCO_3 water type to the mixed (predominantly Na- HCO_3) water type. The softening of the water composition in the

central zone is likely caused by cation exchange where Ca^{2+} in the water exchanges with the Na^+ from the aquifer material. The cation exchange reaction process releases more Na^+ into the groundwater, making it the most abundant cation in the central zone. Other minor water compositions, including Na–Cl, Ca–Cl, Mg–Cl and Ca– HCO_3 , underscore that a mixture of different water compositions from different flow paths is likely to cause the mixed water types observed in this zone. This is corroborated by the factor analysis which revealed three factor models without a dominant process, suggesting that mixed water compositions control groundwater chemistry in the central zone. This is consistent with the general conclusion that the chemical composition of groundwater in the transition zone along the groundwater flow regime is a mixture of different water compositions [64].

In the southern zone, the water composition changes from Na– HCO_3 dominant to a Na–Cl water. The Na–Cl water in the southern zone is most likely derived from two sources. The first source will be the general evolution of anions along the groundwater flow path as described by Chebotarev [64]. According to Chebotarev [64], when water moves through rocks, its chemical composition changes, and the longer the residence time, the more chemically evolved the water becomes. In his theory, the author underlined that along the flow path, HCO_3^- anions dominating the shallow and recharging areas give way to SO_4^{2-} and finally to Cl^- , while Ca^{2+} is displaced by Na^+ . On the other hand, due to the proximity of the southern zone to the sea, it is likely that aerosols from the sea also contribute significantly to the composition of the Na–Cl water. This is confirmed by the factor model (Factor 1) generated for the southern zone, which showed a strong positive correlation with Na^+ , Cl^- and SO_4^{2-} , suggesting a common source which is most likely from marine aerosols consistent with the findings of Tay et al. [19]. The mineralogical composition of the rocks in the study area does not support the possible influence of halite and sulfate minerals, as there is no petrographic evidence in the underlying rocks. In view of this, we could assume that the marine aerosol contribution is likely to influence the hydrochemistry of the southern zone groundwater composition.

5. Conclusions

Understanding the geochemical processes that control the chemical composition of surface water and groundwater is crucial for the development of appropriate water management strategies. In this current study, 90 water samples from rivers and boreholes were analyzed for their chemical parameters, including major ions and trace metals. The hydrochemical data provide the baseline information and was used to assess the quality and infer geochemical processes that control the hydrochemistry of the water resources in the Pra Basin.

Among the two water sources, groundwater is considered good for drinking and irrigation, except for the northern zone, which may require Mn and Fe (total) treatment. Our analysis shows that surface water has poor quality and cannot be used as drinking water in its current state without treatment. The sources of these trace metals could be traced from the underlying geology through water–rock interactions and the illegal mining activities through underground excavations facilitating the dissolution of Mn- and Fe-rich minerals contained in the subsurface materials. Based on the SAR, USSL and the Wilcox indices, all the surface water samples are rated excellent for irrigation. However, the high concentrations of Mn and Fe (total) observed in most of the surface water samples may require treatment to avoid soil acidification and loss of essential soil nutrients. Here we conclude that using only the major ionic composition is not sufficient to determine the drinking and irrigation water quality of surface water and groundwater, and therefore trace metals, such as Mn and Fe (total), as well as toxic metals (mercury, arsenic and cyanide) associated with illegal mining and bacteriological contaminants should be considered for the general water quality assessment.

Water–rock interactions control the chemical composition of groundwater. A combined interpretation of ion ratio plots and statistical analysis underlines that groundwater chemical composition changes with elevation with silicate weathering, carbonate dissolution and

cation exchange as plausible geochemical processes driving the Pra Basin hydrochemistry. Based on the HCA, three distinct chemical associations are recognized, distinguishable by elevation. From this, we could deduce that ground water in the Pra Basin most likely flows in the direction from higher (northern zone) to lower elevations (southern zone). Along the flow regime, the groundwater composition changes from Ca-HCO₃ (northern zone) to a mixed water type dominated by Na-HCO₃ and finally to Na-Cl. The statistical relationship between Na⁺ and Cl⁻ derived from factor analysis indicated a potential influence from marine aerosols since the underlying geology shows no evidence of halite deposits in the area.

This research is part of an ongoing study aimed at conceptualizing the hydrogeochemical conditions in the Pra Basin to aid in water resource management following the pervasive illegal mining activities in and around the study area. As a next step, we plan to implement geochemical models, including inverse and reaction path models, to elucidate the geochemical processes that drive groundwater chemical evolution. In doing so, the reactions of the water with the host rocks can be examined and quantified to understand the chemical behaviour of the dissolved ions in the groundwater system.

Author Contributions: Conceptualization, E.M. and M.K.; methodology, E.M., M.K. and M.D.L.; software, E.M. and M.D.L.; validation, E.M. and M.D.L.; formal analysis, E.M.; investigation, E.M.; writing—original draft predeposits, E.M.; writing—review and editing, E.M., M.D.L. and M.K.; visualization, E.M.; supervision, M.K. All authors have read and agreed to the published version of the manuscript.

Funding: This publication has been supported by the funding programme “Open Access Publikationskosten” Deutsche Forschungsgemeinschaft (DFG, German Research Foundation)—Project Number 491075472.

Data Availability Statement: Datasets related to this article can be found at <https://doi.org/10.5880/GFZ.3.4.2023.002> (accessed on 16 February 2023).

Acknowledgments: This study is part of the first author’s doctoral thesis and he would like to express his greatest appreciation to the German Academic Exchange Service (DAAD) for funding his stay in Germany.

Conflicts of Interest: The authors declare no conflict of interest.

References

1. Katila, P.; Colfer, C.J.P.; De, J.W.; Galloway, G.; Pacheco, P.; Winkel, G. *Sustainable Development Goals*; Cambridge University Press: London, UK, 2019.
2. Groen, J.; Schuchmann, J.; Geirnaert, W. The occurrence of high nitrate concentration in groundwater in villages in Northwestern Burkina Faso. *J. Afr. Earth Sci.* **1988**, *7*, 999–1009. [[CrossRef](#)]
3. Fayiga, A.O.; Ipinmoroti, M.O.; Chirenje, T. Environmental pollution in Africa. *Environ. Dev. Sustain.* **2018**, *20*, 41–73. [[CrossRef](#)]
4. Sasakova, N.; Gregova, G.; Takacova, D.; Mojziso, J.; Papajova, I.; Venglovsky, J.; Szaboova, T.; Kovacova, S. Pollution of surface and ground water by sources related to agricultural activities. *Front. Sustain. Food Syst.* **2018**, *2*, 42. [[CrossRef](#)]
5. Verlicchi, P.; Grillini, V. Surface water and groundwater quality in South Africa and mozambique—Analysis of the Most critical pollutants for drinking purposes and challenges in water treatment selection. *Water* **2020**, *12*, 305. [[CrossRef](#)]
6. Tay, C.K.; Kortatsi, B.K.; Hayford, E.; Hodgson, I.O. Origin of major dissolved ions in groundwater within the Lower Pra Basin using groundwater geochemistry, source-rock deduction and stable isotopes of 2 H and 18 O. *Environ. Earth Sci.* **2014**, *71*, 5079–5097. [[CrossRef](#)]
7. Affum, A.O.; Dede, S.O.; Nyarko, B.J.B.; Acquah, S.O.; Kwaansa-Ansah, E.E.; Darko, G.; Dickson, A.; Affum, E.A.; Fianko, J.R. Influence of small-scale gold mining and toxic element concentrations in Bonsa river, Ghana: A potential risk to water quality and public health. *Environ. Earth Sci.* **2016**, *75*, 178. [[CrossRef](#)]
8. Bempah, C.K.; Ewusi, A. Heavy metals contamination and human health risk assessment around Obuasi gold mine in Ghana. *Environ. Monit. Assess.* **2016**, *188*, 261. [[CrossRef](#)]
9. Armah, F.A.; Quansah, R.; Luginaah, I. A systematic review of heavy metals of anthropogenic origin in environmental media and biota in the context of gold mining in Ghana. *Int. Sch. Res. Not.* **2014**, *3*, 698–714. [[CrossRef](#)]
10. Golow, A.; Mingle, L. Mercury in river water and sediments in some rivers near Dunkwa-on-Offin, an alluvial goldmine, Ghana. *Bull. Environ. Contam. Toxicol.* **2003**, *70*, 0379–0384. [[CrossRef](#)]

11. Amonoo-Neizer, E.H.; Amekor, E. Determination of total arsenic in environmental samples from Kumasi and Obuasi, Ghana. *Environ. Health Perspect.* **1993**, *101*, 46–49. [[CrossRef](#)]
12. Gao, Z.; Wang, Z.; Wang, S.; Wu, X.; An, Y.; Wang, W.; Liu, J. Factors that influence the chemical composition and evolution of shallow groundwater in an arid region: A case study from the middle reaches of the Heihe River, China. *Environ. Earth Sci.* **2019**, *78*, 390. [[CrossRef](#)]
13. Solangi, G.S.; Siyal, A.A.; Siyal, P. Analysis of Indus Delta groundwater and surface water suitability for domestic and irrigation purposes. *Civ. Eng. J.* **2019**, *5*, 1599–1608. [[CrossRef](#)]
14. Ren, X.; Gao, Z.; An, Y.; Liu, J.; Wu, X.; He, M.; Feng, J. Hydrochemical and isotopic characteristics of groundwater in the Jiuquan East Basin, China. *Arab. J. Geosci.* **2020**, *13*, 545. [[CrossRef](#)]
15. Yidana, S.M.; Banoeng-Yakubo, B.; Sakyi, P.A. Identifying key processes in the hydrochemistry of a basin through the combined use of factor and regression models. *J. Earth Syst. Sci.* **2012**, *121*, 491–507. [[CrossRef](#)]
16. Zhang, G.; Deng, W.; Yang, Y.; Salama, R. Evolution study of a regional groundwater system using hydrochemistry and stable isotopes in Songnen Plain, northeast China. *Hydrol. Process. Int. J.* **2007**, *21*, 1055–1065. [[CrossRef](#)]
17. Wang, R.; Bian, J.M.; Gao, Y. Research on hydrochemical spatio-temporal characteristics of groundwater quality of different aquifer systems in Songhua River Basin, eastern Songnen Plain, Northeast China. *Arab. J. Geosci.* **2014**, *7*, 5081–5092. [[CrossRef](#)]
18. Liu, J.; Gao, Z.; Wang, M.; Li, Y.; Ma, Y.; Shi, M.; Zhang, H. Study on the dynamic characteristics of groundwater in the valley plain of Lhasa City. *Environ. Earth Sci.* **2018**, *77*, 646. [[CrossRef](#)]
19. Tay, C.; Hayford, E.; Hodgson, I. Application of multivariate statistical technique for hydrogeochemical assessment of groundwater within the Lower Pra Basin, Ghana. *Appl. Water Sci.* **2017**, *7*, 1131–1150. [[CrossRef](#)]
20. Loh, Y.S.A.; Fynn, O.F.; Manu, E.; Afrifa, G.Y.; Addai, M.O.; Akurugu, B.A.; Yidana, S.M. Groundwater-surface water interactions: Application of hydrochemical and stable isotope tracers to the lake bosumtwi area in Ghana. *Environ. Earth Sci.* **2022**, *81*, 518. [[CrossRef](#)]
21. Loh, Y.S.A.; Addai, M.O.; Fynn, O.F.; Manu, E. Characterisation and quality assessment of surface and groundwater in and around Lake Bosumtwi impact craton (Ghana). *Sustain. Water Resour. Manag.* **2021**, *7*, 81. [[CrossRef](#)]
22. Zhang, B.; Song, X.; Zhang, Y.; Han, D.; Tang, C.; Yu, Y.; Ma, Y. Hydrochemical characteristics and water quality assessment of surface water and groundwater in Songnen plain, Northeast China. *Water Res.* **2012**, *46*, 2737–2748. [[CrossRef](#)] [[PubMed](#)]
23. Xia, C.; Liu, G.; Meng, Y.; Jiang, F. Reveal the threat of water quality risks in Yellow River Delta based on evidences from isotopic and hydrochemical analyses. *Mar. Pollut. Bull.* **2022**, *177*, 113532. [[CrossRef](#)] [[PubMed](#)]
24. Ibrahim, H.; Yaseen, Z.M.; Scholz, M.; Ali, M.; Gad, M.; Elsayed, S.; Khadr, M.; Hussein, H.; Ibrahim, H.H.; Eid, M.H.; et al. Evaluation and prediction of groundwater quality for irrigation using an integrated water quality indices, machine learning models and GIS approaches: A representative case study. *Water* **2023**, *15*, 694. [[CrossRef](#)]
25. Panneerselvam, B.; Ravichandran, N.; Kaliyappan, S.P.; Karuppanan, S.; Bidorn, B. Quality and Health Risk Assessment of Groundwater for Drinking and Irrigation Purpose in Semi-Arid Region of India Using Entropy Water Quality and Statistical Techniques. *Water* **2023**, *15*, 601. [[CrossRef](#)]
26. Loh, Y.S.A.; Akurugu, B.A.; Manu, E.; Aliou, A.S. Assessment of groundwater quality and the main controls on its hydrochemistry in some Voltaian and basement aquifers, northern Ghana. *Groundw. Sustain. Dev.* **2020**, *10*, 100296. [[CrossRef](#)]
27. Okofo, L.B.; Anderson, N.A.; Bedu-Addo, K.; Armoo, E.A. Hydrochemical peculiarities and groundwater quality assessment of the Birimian and Tarkwaian aquifer systems in Bosome Freho District and Bekwai Municipality of the Ashanti Region, Ghana. *Environ. Earth Sci.* **2021**, *80*, 818. [[CrossRef](#)]
28. Yidana, S.M.; Yidana, A. Assessing water quality using water quality index and multivariate analysis. *Environ. Earth Sci.* **2010**, *59*, 1461–1473. [[CrossRef](#)]
29. Commission, W.R. Pra River Basin—Integrated Water Resources Management Plan. 2012. Available online: <https://www.wrc-gh.org/documents/reports/> (accessed on 22 January 2023).
30. Kesse, G.O. *The Mineral and Rock Resources of Ghana*; AA Balkema Publishers: Accord, MA, USA, 1985.
31. Leube, A.; Hirdes, W. The early Proterozoic (Birimian and Tarkwaian) of Ghana and some aspects of its associated gold mineralizations. *Abstr. Gecongress* **1986**, *86*, 315–319.
32. Ganyaglo, S.Y.; Banoeng-Yakubo, B.; Osaе, S.; Dampare, S.B.; Fianko, J.R.; Bhuiyan, M.A. Hydrochemical and isotopic characterisation of groundwaters in the eastern region of Ghana. *J. Water Resour. Prot.* **2010**, *2*, 199. [[CrossRef](#)]
33. Manu, E.; Vieth-Hillebrand, A.; Rach, O.; Schleicher, A.M.; Trumbull, R.; Stammeier, J.A.; Gottsche, A.; Kühn, M. Hydrochemistry and stable oxygen ($\delta^{18}\text{O}$) and hydrogen ($\delta^2\text{H}$) isotopic composition of surface water and groundwater and mineralogy, in the Pra Basin (Ghana) West Africa. *GFZ Data Serv.* **2023**. [[CrossRef](#)]
34. Sahu, P.; Sikdar, P. Hydrochemical framework of the aquifer in and around East Kolkata Wetlands, West Bengal, India. *Environ. Geol.* **2008**, *55*, 823–835. [[CrossRef](#)]
35. WHO. *Guidelines for Drinking-Water Quality*, 4th ed.; Incorporating the First Addendum; World Health Organisation: Geneva, Switzerland, 2017; 541p.
36. Allison, L.E.; Richards, L.A. *Diagnosis and Improvement of Saline and Alkali Soils*; Number 60; Soil and Water Conservative Research Branch, Agricultural Research Service: Washington, DC, USA, 1954.
37. Hem, J.D. *Study and Interpretation of the Chemical Characteristics of Natural Water*; Department of the Interior, US Geological Survey: Washington, DC, USA, 1985; Volume 2254.

38. Schoeller, H. Qualitative evaluation of groundwater resources. In *Methods and Techniques of Groundwater Investigations and Development*; UNESCO: Paris, France, 1965; Volume 54–83.
39. Kaiser, H.F. The application of electronic computers to factor analysis. *Educ. Psychol. Meas.* **1960**, *20*, 141–151. [[CrossRef](#)]
40. Yidana, S.M.; Dzikunoo, E.A.; Aliou, A.S.; Adams, R.M.; Chagbeleh, L.P.; Anani, C. The geological and hydrogeological framework of the Panabako, Kodjari, and Bimbilla formations of the Voltaian supergroup—Revelations from groundwater hydrochemical data. *Appl. Geochem.* **2020**, *115*, 104533. [[CrossRef](#)]
41. Statistics, I. *IBM SPSS Statistics for Windows*; Version 22.0; IBM Corp: Armonk, NY, USA, 2013.
42. Ward, J.H., Jr. Hierarchical grouping to optimize an objective function. *J. Am. Stat. Assoc.* **1963**, *58*, 236–244. [[CrossRef](#)]
43. Güler, C.; Thyne, G.D. Hydrologic and geologic factors controlling surface and groundwater chemistry in Indian Wells–Owens Valley area, southeastern California, USA. *J. Hydrol.* **2004**, *285*, 177–198. [[CrossRef](#)]
44. Wilcox, L. *Classification and Use of Irrigation Waters*; Number 969; US Department of Agriculture: Washington, DC, USA, 1955.
45. Wang, S. Hydrochemical and isotopic characteristics of groundwater in the Yanqi Basin of Xinjiang province, northwest China. *Environ. Earth Sci.* **2014**, *71*, 427–440. [[CrossRef](#)]
46. Piper, A.M. A graphic procedure in the geochemical interpretation of water-analyses. *Eos Trans. Am. Geophys. Union* **1944**, *25*, 914–928. [[CrossRef](#)]
47. Gibbs, R.J. Mechanisms controlling world water chemistry. *Science* **1970**, *170*, 1088–1090. [[CrossRef](#)] [[PubMed](#)]
48. Drever, J.I. *The Geochemistry of Natural Waters*; Prentice Hall: Englewood Cliffs, NJ, USA 1988; Volume 437.
49. Appelo, C.A.J.; Postma, D. *Geochemistry, Groundwater and Pollution*; CRC Press: London, UK, 2004.
50. Manu, J.; Hayford, E.; Anani, C.; Kutu, J.M.; Armah, T. Aspects of the chemical composition of the Birimian gold fluid. *J. Earth Sci. Geotech. Eng.* **2013**, *3*, 87–106.
51. Bessah, E.; Raji, A.O.; Taiwo, O.J.; Agodzo, S.K.; Ololade, O.O.; Strapasson, A.; Donkor, E. Assessment of surface waters and pollution impacts in Southern Ghana. *Hydrol. Res.* **2021**, *52*, 1423–1435. [[CrossRef](#)]
52. Darko, H.F.; Karikari, A.Y.; Duah, A.A.; Akurugu, B.A.; Mante, V.; Teye, F.O. Effect of small-scale illegal mining on surface water and sediment quality in Ghana. *Int. J. River Basin Manag.* **2021**. [[CrossRef](#)]
53. Ayers, R.S.; Westcot, D.W. *Water Quality for Agriculture*; Food and Agriculture Organization of the United Nations Rome: Rome, Italy, 1985; Volume 29.
54. Grabić, J.; Vranešević, M.; Zemunac, R.; Bubulj, S.; Bezdan, A.; Ilić, M. Iron and Manganese in Well Water: Potential Risk for Irrigation Systems. *Acta Hort. Regiotech.* **2019**, *22*, 93–96. [[CrossRef](#)]
55. Anku, Y.S.; Banoeng-Yakubo, B.; Asiedu, D.K.; Yidana, S.M. Water quality analysis of groundwater in crystalline basement rocks, Northern Ghana. *Environ. Geol.* **2009**, *58*, 989–997. [[CrossRef](#)]
56. Yidana, S.M.; Banoeng-Yakubo, B.; Aliou, A.S.; Akabzaa, T.M. Groundwater quality in some Voltaian and Birimian aquifers in northern Ghana—Application of multivariate statistical methods and geographic information systems. *Hydrol. Sci. J.* **2012**, *57*, 1168–1183. [[CrossRef](#)]
57. Koffi, K.V.; Obuobie, E.; Banning, A.; Wohnlich, S. Hydrochemical characteristics of groundwater and surface water for domestic and irrigation purposes in Veve catchment, Northern Ghana. *Environ. Earth Sci.* **2017**, *76*, 185. [[CrossRef](#)]
58. Chegbeleh, L.P.; Akurugu, B.A.; Yidana, S.M. Assessment of Groundwater Quality in the Talensi District, Northern Ghana. *Sci. World J.* **2020**, *2020*, 8450860. [[CrossRef](#)]
59. Kaka, E.; Akiti, T.; Nartey, V.; Bam, E.; Adomako, D. Hydrochemistry and evaluation of groundwater suitability for irrigation and drinking purposes in the southeastern Volta River basin: Many Krobo area, Ghana. *Elixir Agric.* **2011**, *39*, 4793–4807.
60. Gibrilla, A.; Bam, E.; Adomako, D.; Ganyaglo, S.; Osae, S.; Akiti, T.; Kebede, S.; Achoribo, E.; Ahiale, E.; Ayanu, G.; et al. Application of water quality index (WQI) and multivariate analysis for groundwater quality assessment of the Birimian and Cape Coast Granitoid Complex: Densu River Basin of Ghana. *Water Qual. Expo. Health* **2011**, *3*, 63–78. [[CrossRef](#)]
61. Banks, D.; Frengstad, B. Evolution of groundwater chemical composition by plagioclase hydrolysis in Norwegian anorthosites. *Geochim. Cosmochim. Acta* **2006**, *70*, 1337–1355. [[CrossRef](#)]
62. Meybeck, M. Global chemical weathering of surficial rocks estimated from river dissolved loads. *Am. J. Sci.* **1987**, *287*, 401–428. [[CrossRef](#)]
63. Freeze, R.A.; Cherry, J. *Groundwater*; Prentice-Hall, Inc.: Englewood Cliffs, NJ, USA, 1979.
64. Chebotarev, I. Metamorphism of natural waters in the crust of weathering—1. *Geochim. Cosmochim. Acta* **1955**, *8*, 22–48. [[CrossRef](#)]
65. Nude, P.; Hanson, J.; Dampare, S.; Akiti, T.; OsAE, S.; Nyarko, E.; Zkaria, N.; Enti-Brown, S. Geochemistry of Pegmatites associated with the cape coast granite complex in the Egyaa and Akim Oda areas of southern Ghana. *Ghana J. Sci.* **2011**, *51*, 89–100.

Disclaimer/Publisher’s Note: The statements, opinions and data contained in all publications are solely those of the individual author(s) and contributor(s) and not of MDPI and/or the editor(s). MDPI and/or the editor(s) disclaim responsibility for any injury to people or property resulting from any ideas, methods, instructions or products referred to in the content.